



Liverpool John Moores University

Point Cloud Registration of non-rigid objects in sparse 3D Scans with applications in Mixed Reality

by

Manorama Jha

A thesis submitted in partial fulfillment for the
degree of Master of Science

in

Artificial Intelligence and Machine Learning

at the

School of Computer Science and Mathematics

December 2022

Declaration

The work presented in this thesis was carried out at the School of Computer Science and Mathematics, Liverpool John Moores University. Unless otherwise stated, it is the original work of the author.

While registered as a candidate for the degree of Master of Science in Artificial Intelligence and Machine Learning, for which submission is now made, the author has not been registered as a candidate for any other award. This thesis has not been submitted in whole, or in part, for any other degree.

MANORAMA JHA

School of Computer Science and Mathematics

Liverpool John Moores University

James Parsons Building

3 Byrom Street

Liverpool

Merseyside

L3 3AF

UK

DECEMBER 2022

Abstract

Point Cloud Registration is the problem of aligning the corresponding points of two 3D point clouds referring to the same object. The challenges include dealing with noise and partial match of real-world 3D scans. For non-rigid objects, there is an additional challenge of accounting for deformations in the object shape that happen to the object in between the two 3D scans. In this project, we study the problem of non-rigid point cloud registration for use cases in the Augmented/Mixed Reality domain. We focus our attention on a special class of non-rigid deformations that happen in rigid objects with parts that move relative to one another about joints, for example, robots with hands and machines with hinges. We propose an efficient and robust point-cloud registration workflow for such objects and evaluate it on real-world data collected using Microsoft Hololens 2, a leading Mixed Reality Platform.

Acknowledgements

I would like to take this opportunity to thank all the people and organizations that have played a critical role in making this thesis a reality. Right at the beginning, I would like to thank GridRaster Inc. for providing me with a rare opportunity to carry out research at this wonderful intersection of Mixed Reality and Artificial Intelligence. I would like to especially thank my wonderful mentors from GridRaster – Rishi, Pradeep, Bhaskar, Yiyong, Dijam and Sita – for constantly supporting me in my job and encouraging me to pursue academic research.

I would like to thank my parents - Nityananda Jha and Ranjana Jha for going against all odds to support my education and well-being. I would like to thank my little brother Harimohan Jha for being my support system and always cheering me up when the time is low.

I would like to thank Prof. Pabitra Mitra and Prof. Jhareshwar Maiti at Indian Institute of Technology Kharagpur for introducing me to the world of Extended Reality. Without their kind support, it would not have been possible for me to build a career in Mixed Reality. I would also like to thank my mentor and friend Anirban Santara for helping me build a research portfolio in the early days of my career.

My life would be meaningless without my dear friends Anjali Sharma, Junmoni Boroghain and Khushi Gangireddy. I would like to thank them for being there for me and giving me hope when I could not find a reason to push on by myself.

Declaration of Authorship

I, **Manorama Jha**, declare that this thesis titled, "**Point Cloud Registration of non-rigid objects in sparse 3D Scans with applications in Mixed Reality**" and the work presented in it are my own. I confirm that:

- This work was done wholly or mainly while in candidature for a research degree at this University.
- Where any part of this thesis has previously been submitted for a degree or any other qualification at this University or any other institution, this has been clearly stated.
- Where I have consulted the published work of others, this is always clearly attributed.
- Where I have quoted from the work of others, the source is always given. With the exception of such quotations, this thesis is entirely my own work.
- I have acknowledged all main sources of help.
- Where the thesis is based on work done by myself jointly with others, I have made clear exactly what was done by others and what I have contributed myself.

Signed: Manorama Jha

Date: 07.12.2022

“ DREAM, DREAM, DREAM - Till your dreams come true :) ”

Liverpool John Moores University

Abstract

Artificial Intelligence and Machine Learning
School of Computer Science and Mathematics

Master of Science

by Manorama Jha

Point Cloud Registration is the problem of aligning the corresponding points of two 3D point clouds referring to the same object. The challenges include dealing with noise and partial match of real-world 3D scans. For non-rigid objects, there is an additional challenge of accounting for deformations in the object shape that happen to the object in between the two 3D scans. In this project, we study the problem of non-rigid point cloud registration for use cases in the Augmented/Mixed Reality domain. We focus our attention on a special class of non-rigid deformations that happen in rigid objects with parts that move relative to one another in joints, for example, robots with hands and machines with hinges. We propose an efficient and robust point-cloud registration workflow for such objects and evaluate it on real-world data collected using Microsoft HoloLens 2, a leading Mixed Reality Platform.

Contents

Declaration	ii
Abstract	iii
Acknowledgements	iv
Declaration of Authorship	v
Abstract	vii
List of Figures	xii
List of Tables	xv
Abbreviations	xvi
1 Introduction	1
Introduction	1
1.1 Background	2
1.1.1 Mixed Reality (MR)	2
1.1.2 MR Headsets	2
1.1.3 Engineering Challenges faced by MR	3
1.2 Problem Statement	4
1.3 Aims and Objectives	4
1.4 Research Questions	5
1.5 Scope of the Study	5
1.6 Significance of the Study	5
1.7 Organization of the Thesis	6
1.8 Conclusion	7
2 Literature Review	8
Literature Review	8

2.1	Introduction	8
2.2	Point Cloud Registration	8
2.2.1	Feature extraction	9
2.2.2	Feature matching and registration	11
2.2.2.1	Rigid Registration	11
2.2.2.2	Non-rigid registration	11
2.2.3	Challenges	12
2.2.3.1	Lack of ordering or structure	12
2.2.3.2	Sparsity	12
2.2.3.3	Noise and Outliers	12
2.2.3.4	Partial Overlap	13
2.3	Conclusion	14
3	Research Methodology	15
	Research Methodology	15
3.1	Introduction	15
3.2	Research Tools	15
3.2.1	Hardware	15
3.2.1.1	Data capture devices	16
3.2.1.2	Data processing devices	16
3.2.1.3	Data rendering devices	16
3.2.2	Software	17
3.3	Datasets for our Study	17
3.4	Data Visualisation	19
3.5	Training Objectives	20
3.6	Evaluation Metrics	21
3.7	Baseline Selection	21
3.8	Conclusion	23
4	Non-Rigid Point Cloud Registration	24
	Non-Rigid Point Cloud Registration	24
4.1	Introduction	24
4.2	Lepard: Learning partial point cloud matching in rigid and de- formable scenes	25
4.2.1	Notation	26
4.2.2	Local geometry feature extraction	26
4.2.2.1	Kernel Point Convolution	26
4.2.3	Relative 3D Positional Encoding	28
4.2.4	Transformer	29
4.2.4.1	Self Attention Layer	29
4.2.4.2	Cross Attention Layer	29
4.2.5	Position-aware Feature Matching	30
4.2.6	Rigid Fitting with Soft Prucrustes	30

4.3	Non-rigid Registration	31
4.3.1	Non-rigid Iterative Closest Point (N-ICP)	31
4.4	Conclusion	32
5	Proposed Method	33
	Proposed Method	33
5.1	Introduction	33
5.2	Motivation	33
5.3	Challenges	34
5.4	Our approach	34
5.4.0.1	Graph representation of source	36
5.4.0.2	Correspondence matching using Lepard	37
5.4.0.3	Whole body rigid fitting	37
5.4.0.4	Part-wise tuning	38
5.4.1	Final Result	42
5.5	Addressing the challenges	42
5.6	Conclusion	43
6	Results and Discussion	44
	Results and Discussion	44
6.1	Introduction	44
6.2	Experimental Setup	44
6.2.1	Code base	44
6.2.2	Data collection	45
6.2.3	Data preparation	46
6.3	Results	47
6.3.1	Experiment 1: No deformations, low noise	47
6.3.1.1	Discussion	47
6.3.2	Experiment 2: Non-rigid deformation in one part, low noise	48
6.3.2.1	Discussion	51
6.3.3	Experiment 3: Non-rigid deformation in multiple parts, low noise	51
6.3.3.1	Discussion	53
6.3.4	Experiment 4: Non-rigid deformation in multiple parts, Noisy target point cloud	56
6.3.4.1	Discussion	57
6.4	Hyperparameter values	57
6.5	Conclusion	58
7	Conclusion	62
	Conclusion	62
7.1	Introduction	62

7.2	Summary of achievements	62
7.3	Contribution to knowledge	63
7.4	Recommendations for future work	63
A	Research Proposal	74
A.1	Summary of the Proposed Research	76
A.2	Research Question	76
A.3	Aim and Objectives	76
A.4	Background	77
A.4.1	Mixed Reality	77
A.4.1.1	Introduction	77
A.4.1.2	MR Headsets	78
A.4.1.3	Challenges	78
A.4.2	Point Cloud Registration	79
A.4.2.1	Introduction	79
A.4.2.2	Approaches to Solution	79
A.4.2.3	Challenges	82
A.5	Problem Statement	83
A.5.1	Definition	83
A.5.2	Robust real-world performance	84
A.6	Methodology	84
A.6.1	Baseline Algorithm	84
A.6.2	Training Objectives	85
A.6.3	Evaluation Metrics	85
A.6.4	Datasets	85
A.6.5	Real World Evaluation	86
A.7	Expected Outcome	86
A.8	Required Resources	87
A.8.1	Hardware	87
A.8.2	Software	88
A.9	Plan of Work	88
A.9.1	Contingency Plan	88

List of Figures

1.1	Microsoft HoloLens 2, the Mixed Reality platform used in our study.	3
2.1	Kernel Point Convolution (Thomas et al., 2019) (KPConv) demonstrated on 2D points.	10
2.2	Example of sparse point cloud scan	13
2.3	Example of noise in point clouds scanned by Microsoft HoloLens 2.	13
2.4	Example of partial overlap between the source and target point clouds	14
3.1	Kernel Sample data point from 3DMatch dataset.	18
3.2	Sample data point from 3DLoMatch dataset.	18
3.3	Samples from the 4DMatch/4DLoMatch dataset. The top row shows the input source and target point clouds and the bottom row shows the ground truth registration outcomes. The percentages at the bottom of the figure denote the percentage of overlap between the source and target point clouds in each of these examples.	19
3.4	Real-world objects used for our study. (Left) Cubebot robot model (non-rigid). (Right) NASA Lander model (rigid)	19
3.5	Real-world environment (cluttered) used in our tests.	20
3.6	Point cloud scan of the real-world cluttered test environment. Scan generated using Microsoft HoloLens 2.	20
3.7	Illustration of the Inlier Ratio (IR) metric.	21
3.8	Illustration of the Non-rigid Feature Matching Recall (NFMR) metric	22
3.9	Flowchart depicting the architecture of Lepard. Please refer to the paper (Li & Harada, 2022) for details.	22
5.1	NASA Viking Lunar Lander with parts labelled. We show two views to reveal the 3D shape of the model.	36
5.2	Source and target point clouds in the example that we use to describe our workflow in this section.	36
5.3	Graph Construction of NASA Viking Lunar Lander labelled	37
5.4	Point Cloud of NASA Viking Lunar Lander Source and target after Rigid fitting	37
5.5	Correspondences of Dish-pole of NASA Viking Lunar Lander . . .	38
5.6	Correspondences of partial antenna and leg3 of NASA Viking Lunar Lander	39
5.7	Correspondences of the dish of NASA Viking Lunar Lander	39
5.8	Correspondences of leg 1 of NASA Viking Lunar Lander	40

5.9	Diagram showing how we compute the region of interest	41
5.10	Results: Left - After RANSAC, Right - After ICP	41
5.11	Final Result after ICP	42
6.1	CAD Model of NASA Viking Lander used as source point cloud in our experiments.	45
6.2	CAD Model of dancing Cubebot used as source point cloud in our experiments.	46
6.3	Cubebot with parts labelled.	46
6.4	Pipeline for converting data recorded with Microsoft HoloLens 2 into the input format of Lepard.	47
6.5	Source and target point clouds for Experiment 1 in Section 6.3.1 with NASA Viking Lander.	48
6.6	Transformed source and target point clouds for Experiment 1 in Section 6.3.1 with NASA Viking Lander.	48
6.7	Visualization alignment of transformed source and target point clouds for Experiment 1 in Section 6.3.1 with NASA Viking Lander. C2C distance is a cloud-to-cloud approximate nearest neighbor distance computed by CloudCompare (Girardeau-Montaut, 2016).	49
6.8	Source and target point clouds for Experiment 1 in Section 6.3.1 with Cubebot.	49
6.9	Transformed source and target point clouds for Experiment 1 in Section 6.3.1 with Cubebot.	50
6.10	Visualization alignment of transformed source and target point clouds for Experiment 1 in Section 6.3.1 with Cubebot. C2C distance is a cloud-to-cloud approximate nearest neighbour distance computed by CloudCompare (Girardeau-Montaut, 2016).	50
6.11	Source and target point clouds for Experiment 2 in Section 6.3.2 with NASA Viking Lander.	51
6.12	Transformed source and target point clouds for Experiment 2 in Section 6.3.2 with NASA Viking Lander.	52
6.13	Visualization alignment of transformed source and target point clouds for Experiment 2 in Section 6.3.2 with NASA Viking Lander. C2C distance is a cloud-to-cloud approximate nearest neighbor distance computed by CloudCompare (Girardeau-Montaut, 2016).	52
6.14	Source and target point clouds for Experiment 2 in Section 6.3.2 with Cubebot.	53
6.15	Transformed source and target point clouds for Experiment 2 in Section 6.3.2 with Cubebot.	53
6.16	Visualization alignment of transformed source and target point clouds for Experiment 2 in Section 6.3.2 with Cubebot. C2C distance is a cloud-to-cloud approximate nearest neighbor distance computed by CloudCompare (Girardeau-Montaut, 2016).	54
6.17	Source and target point clouds for Experiment 3 in Section 6.3.3 with NASA Viking Lander.	54

6.18	Transformed source and target point clouds for Experiment 3 in Section 6.3.3 with NASA Viking Lander.	55
6.19	Visualization alignment of transformed source and target point clouds for Experiment 3 in Section 6.3.3 with NASA Viking Lander. C2C distance is a cloud-to-cloud approximate nearest neighbor distance computed by CloudCompare (Girardeau-Montaut, 2016).	55
6.20	Source and target point clouds for Experiment 3 in Section 6.3.3 with Cubebot.	56
6.21	Transformed source and target point clouds for Experiment 3 in Section 6.3.3 with Cubebot.	56
6.22	Visualization alignment of transformed source and target point clouds for Experiment 3 in Section 6.3.3 with Cubebot. C2C distance is a cloud-to-cloud approximate nearest neighbour distance computed by CloudCompare (Girardeau-Montaut, 2016).	57
6.23	Source and target point clouds for Experiment 4 in Section 6.3.4 with NASA Viking Lander.	58
6.24	Transformed source and target point clouds for Experiment 4 in Section 6.3.4 with NASA Viking Lander.	58
6.25	Visualization alignment of transformed source and target point clouds for Experiment 4 in Section 6.3.4 with NASA Viking Lander. C2C distance is a cloud-to-cloud approximate nearest neighbour distance computed by CloudCompare (Girardeau-Montaut, 2016).	59
6.26	Source and target point clouds for Experiment 4 in Section 6.3.4 with Cubebot.	59
6.27	Transformed source and target point clouds for Experiment 4 in Section 6.3.4 with Cubebot.	60
6.28	Visualization alignment of transformed source and target point clouds for Experiment 4 in Section 6.3.4 with Cubebot. C2C distance is a cloud-to-cloud approximate nearest neighbour distance computed by CloudCompare (Girardeau-Montaut, 2016).	60
A.1	Microsoft HoloLens 2, the Mixed Reality platform used in our study.	78
A.2	Example of sparse point cloud scan	82
A.3	Example of noise in point clouds scanned by Microsoft HoloLens 2.	83
A.4	Example of partial overlap between the source and target point clouds	84
A.5	Real-world objects used for our study. (Left) Cubebot robot model. (Right) Viking NASA Lander model.	86
A.6	Real-world environment (cluttered) used in our tests.	87

List of Tables

6.1	Table of hyperparameters.	58
A.1	Gantt Chart showing the plan of work for this thesis.	88

Abbreviations

PCR	P oint C loud R egistration
MR	M ixed R eality
HMD	H ead M ounted D isplay
RGB	R ed G reen B lue
IMU	I ntertial M easurement U nit
3D	3 - D imensional
GPU	G raphics P rocessing U nit
FPGA	F ield P rogrammable G ate A rray
UX	U ser E xperience
XR	E xtended R eality
MRI	M agnetic R esonance I maging
CT	S can C omputed T omography S can
2D-CNN	C onvolutional N eural N etworks
3D-CNN	C onvolutional N eural N etworks
MLP	M ulti L ayer P erceptron
KPConv	K ernel P oint C onvolution
2D	2 - D imensional
RANSAC	R ANdom S Ample C onsensus
ICP	I terative C losest P oint
MP	M ega P ixel
CAD	C omputer A ided D esign
SLAM	S imultaneous L ocalization A nd M apping ()
IR	I nliter R atio
NFMR	N on-rigid F eature M atching R ecall

KPFCN	F ully C onvolutional N eural N etwork
KNN	K -Nearest N eighbor
N-ICP	N on- R igid I terative C losest P oint
NASA	N ational A eronautics and S pace A dministration

...

Chapter 1

Introduction

In this thesis, we study the problem of Alignment in Mixed Reality with a special focus on deformable or non-rigid objects. The problem of Alignment in Mixed Reality is synonymous with the problem of Point Cloud Registration (PCR) in Computer Vision. PCR entails finding a spatial transformation function that maps a source point cloud to a target point cloud (usually of the same object or scene as the source, but displaced or deformed) such that the corresponding points superimpose. PCR has numerous practical applications in a wide range of fields including design, manufacturing, and medicine. For example, for repairing a precision-engineered component in a damaged aircraft, being able to overlay a reference model of the component on the real instance would be of immense help to the technicians. PCR is performed in two steps - a) Correspondence Matching: determining matching pairs of points in the two-point clouds, and b) Transformation Prediction: estimating the transformation function that would register the corresponding points in both point clouds. Although the problem of point-cloud registration has been studied extensively in the case of rigid objects, it still remains a topic of extensive research for non-rigid objects. In real-world applications point cloud scans are seldom clean. For such conditions, a common challenge is dealing with noisy point clouds and only partial matches between the source and target point clouds. In this thesis, we will study the problem of point cloud registration for non-rigid objects in the presence of noise and partial match.

1.1 Background

In this section, we will briefly introduce the topic of Mixed Reality that forms the foundation of this thesis.

1.1.1 Mixed Reality (MR)

In the digital age of today, we humans and almost all things we interact with on a daily basis have a digital self in addition to physical existence. Mixed Reality (MR) is the idea of creating an immersive and seamless experience by blending digital entities in a real-world environment. Mixed reality applications can render accurate to-scale digital models of objects — both static and dynamic — and allow the user to interact with them using intuitive gestures that resemble the way they would interact with the real object. High-precision physics simulation allows accurate reproduction of real-world outcomes of these interactions — thus providing a highly capable tool for education, design, and planning. Mixed reality is also capable of virtual teleportation of human users by mapping their actions and expressions on virtual avatars, thus taking remote collaboration to a whole new level. Mixed reality tools are set to revolutionize engineering, design, productivity, education, and entertainment. This makes mixed reality one of the most actively researched areas of computer science at the moment.

1.1.2 MR Headsets

The most important hardware component of a Mixed Reality system is the Head Mounted Display (HMD) or Headset. Some popular examples are Microsoft HoloLens ([Ungureanu et al., 2020](#)) and Magic Leap. Mixed Reality headsets have a transparent visor through which the user can see the world and different kinds of optics and display elements that project the virtual objects in the field of view of the user. An elaborate set of RGB cameras and laser scanners is used for spatial mapping, localization, and tracking. MR headsets also have an Inertial Measurement Unit (IMU) consisting of an accelerometer, a magnetometer, and a gyroscope that tracks the movement of the user's head through space in six degrees of freedom. Figure [1.1](#) shows the components of Microsoft HoloLens 2, the MR

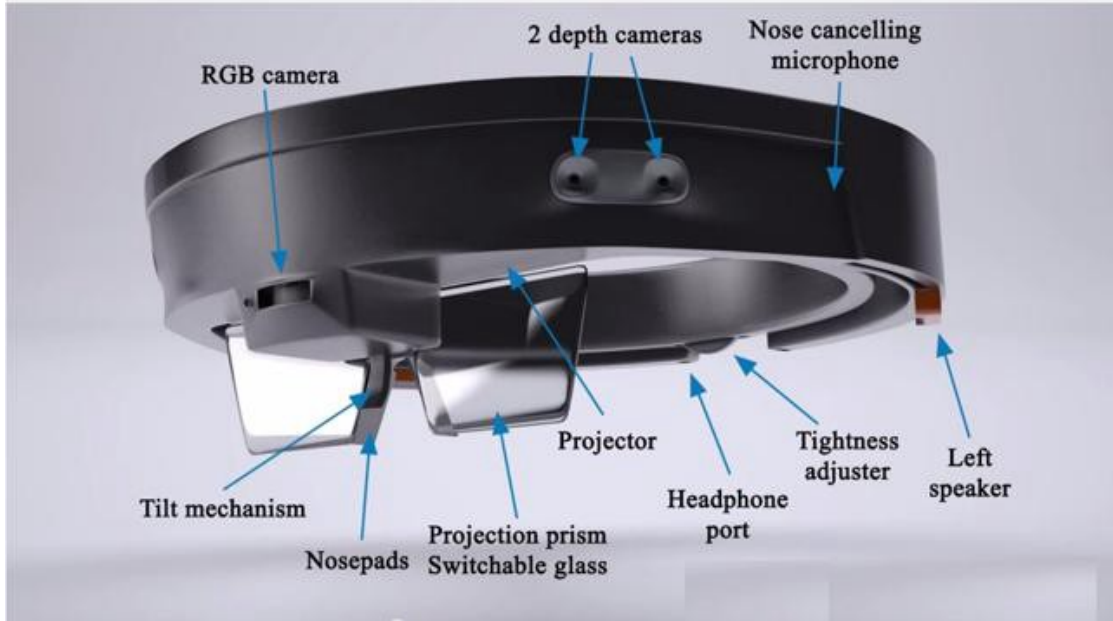


FIGURE 1.1: Microsoft HoloLens 2, the Mixed Reality platform used in our study.

headset that we plan to use in this thesis. MR Headsets provide multi-modal user interfaces that combine head gestures, voice commands, and eye gaze.

1.1.3 Engineering Challenges faced by MR

MR headsets must be power efficient, lightweight and ergonomic. Spatial mapping using multiple modalities, scene reconstruction, gesture recognition, voice recognition, and high-polygon rendering are some primary tasks that are at the core of most Mixed Reality experiences. These 3D Computer Vision and Computer Graphics tasks are compute-intensive and the limited on-device resources are not adequate for achieving these at a latency low enough for supporting an immersive MR experience. To mitigate this issue, most MR platforms employ a hybrid architecture where the compute-intensive tasks like those involving deep neural networks and rendering are off-loaded to high-performance and specialized hardware (e.g. GPU, FPGA) in the cloud, and the on-board hardware is used only for encoding-decoding of data, communication with the cloud and interactions with the user (UX).

1.2 Problem Statement

In this project, we aim to study the problem of non-rigid partial point cloud registration for Mixed Reality applications. Mixed Reality (MR) is transforming the industry by providing unique opportunities in engineering design, remote operations, and collaboration. We specifically intend to implement a state-of-the-art point cloud registration algorithm - Lepard (Li & Harada, 2022) - on Microsoft HoloLens 2 Mixed Reality Platform (Ungureanu et al., 2020) and investigate potential causes of drift and latency bottlenecks in real-world MR use cases. The anticipated outcomes of this research project are a detailed account of failure modes of Lepard and related algorithms and a robust and fast inference pipeline that is robust to outliers and noise in real-life 3D scans and capable of supporting real-time Mixed Reality applications.

1.3 Aims and Objectives

In this thesis, we aim to study the problem of 3D Point Cloud Registration for non-rigid objects. Apart from wide-spread relevance in computer vision, robotics, and medical science, this problem statement is central in many Mixed Reality applications. Although significant advancements have been made in 3D representation learning and computer vision in recent years, several engineering challenges stand in the way of deploying these algorithms at scale. The objectives of this thesis are as follows:

- Prepare a thorough literature review of prominent approaches to 3D Point Cloud Registration with emphasis on non-rigid objects and relevance in Mixed Reality.
- Implement the current state-of-the-art algorithm - Lepard (Li & Harada, 2022) - on the industry-leading Mixed Reality platform - Microsoft HoloLens 2 (Ungureanu et al., 2020).
- Evaluate real-time 3D point cloud registration for deformable and non-deformable objects in uncontrolled real-world settings in the presence and absence of distraction and with varying levels of noise in the 3D scans.

- Identify and mitigate any causes of drift or misalignment and potential bottlenecks slowing down the inference pipeline.

1.4 Research Questions

In this thesis we will address the following research question:

“Can we make state-of-the-art non-rigid point cloud registration algorithms robust and low-latency for Mixed Reality use cases in real-world environments?”

1.5 Scope of the Study

In this thesis, we will focus on the problem of non-rigid point cloud registration only. Although we use models trained on public benchmark PCR datasets, the focus of this thesis is to achieve high performance on scans collected using the mixed reality platform - Microsoft Hololens 2. We want to focus on objects that are composed of rigid parts that can move relative to one another (about a hinge, for example). Such objects are very common in enterprise mixed reality applications. Machine parts, doors, drawers and antennas are a few examples. We will only consider the most recent state-of-the-art method Leopard ([Li & Harada, 2022](#)) as our baseline.

1.6 Significance of the Study

Mixed Reality (MR) is a form of eXtended Reality (XR) that allows the user to render and interact with virtual 3D holograms in a real-world environment [[\(Speicher et al., 2019\)](#), [\(Rokhsaritalemi et al., 2020\)](#)]. In an interior design use case, MR would allow the user to render the hologram of a couch in an empty room and move it around the room with hand gestures [[\(Huang et al., 2018\)](#)] to find out where in the room it would look best [[\(Kent et al., 2021\)](#), [\(Jain & Werth, 2019\)](#)]. One of the primary use cases of this technology is to overlay or register a virtual reference model of an object on top of a real instance of the same object for comparison. For example, in manufacturing, a virtual reference model of a

precision engineering part can be overlaid on a damaged instance for inspection, repair [(Abate et al., 2013), (Borsci et al., 2015)] and training [(Mueller & Ferreira, 2003), (Kirkley & Kirkley, 2005), (Wang et al., 2004)]. In remote assistance, a circuit diagram can be overlaid on a real switchboard and remote instructions can be issued for debugging the connections (Ladwig & Geiger, 2018). In surgery, pre-operative scans (like MRI, CT Scan, etc.) can be overlaid on the patient’s organ in real-time for precise guidance to the point of surgery (Chen et al., 2017).

1.7 Organization of the Thesis

The thesis is organized as follows:

- In order to carry out research on non-rigid point cloud registration it is crucial to build a strong understanding of the foundational concepts and algorithms. In Chapter 2, we describe different point cloud registration workflows and present a detailed survey of the literature in this field. It is also important to understand the challenges involved in this real world applications of these methods and we also discuss these in the same chapter.
- Point cloud registration is a vast area of computer vision and it is important to scope the problems studied in this Masters’ thesis. In Chapter 3, we chart out the questions that we aim to address in this thesis. We also describe the datasets, tools, and compute resources that we use in our study.
- As a primer to the proposed methods, we present a detailed account of the prior work that our proposed algorithm is based off in Chapter 4. We identify the drawbacks of these methods when it comes to the application of our interest and set the stage for the presentation of our original contributions.
- Finally, in Chapter 5, we present our algorithm for non-rigid registration of rigid objects with moving parts.
- In Chapter 6, we present a detailed experimental study of real world evaluation of our proposed approach.
- We conclude the thesis in Chapter 7 with a summary of our contributions and recommended directions for future work.

1.8 Conclusion

In this section, we introduced the problem statement studied in this thesis. We articulated our aims and objectives and research questions to be addressed. We also described the scope, significance and structure of this study.

Chapter 2

Literature Review

2.1 Introduction

In the previous chapter, we introduced the problem of point cloud registration and explained the motivation of this thesis - point cloud registration. This chapter presents a review of point cloud registration algorithms. We also discuss the challenges of this task and ways in which people have approached a solution.

2.2 Point Cloud Registration

Point cloud registration, also called Alignment (in MR jargon), is the task of finding a spatial transformation (such as rotation, translation and scaling) which when applied to a source point cloud results in point-wise superposition with a destination point cloud of the same object/scene. These algorithms fall in two categories - rigid and non-rigid - depending on whether deformations in the object/scene between the two scans can be addressed.

The general approach to point-cloud registration involves two steps: a) feature extraction, and b) feature matching and registration.

2.2.1 Feature extraction

Each point in a point cloud must be assigned a feature vector representing its 3D position and context including local geometry, color and texture [Weinmann et al. \(2017\)](#). The first step is to define a neighborhood for each point. Some common examples are spherical [Lee & Schenk \(2002\)](#), [Linsen & Prautzsch \(2001\)](#) or cylindrical [Filin & Pfeifer \(2005\)](#), [Niemeyer et al. \(2014\)](#) neighborhoods parameterized by radius [Lee & Schenk \(2002\)](#), [Filin & Pfeifer \(2005\)](#) or the number of nearest neighbours by Euclidean distance [Linsen & Prautzsch \(2001\)](#), [Niemeyer et al. \(2014\)](#). These parameters give us the means to control the scale at which local 3D structures must be encoded. The value of the scale parameter is usually chosen using prior knowledge [Weinmann et al. \(2015\)](#) or learned from data [Weinmann et al. \(2015\)](#), [Mitra & Nguyen \(2003\)](#), [Lalonde et al. \(2005\)](#) [Demantké et al. \(2011\)](#) and multi-scale approaches are also popular [Niemeyer et al. \(2014\)](#), [Brodu & Lague \(2012\)](#), [Schmidt et al. \(2014\)](#). Once a neighbourhood of a point is defined, feature extraction encodes the local 3D geometry to attach semantics or context to the point. Certain shape primitives can be obtained by computing the eigenvalues of a 3D structure tensor constructed using the spatial coordinates of neighbouring points [Jutzi & Gross \(2009\)](#), [West et al. \(2004\)](#), [Pauly et al. \(2003\)](#). Other features that are extracted are angular characteristics [Munoz et al. \(2009\)](#), height [Mallet et al. \(2011\)](#), moments [Hackel et al. \(2016\)](#), surface properties, slope, vertical profiles and 2D projections [Guo et al. \(2015\)](#), shape distributions [Osada et al. \(2002\)](#), [Blomley et al. \(2016\)](#), and point-feature histograms [Rusu et al. \(2009\)](#).

Modern approaches use Deep Neural Network ([Goodfellow et al., 2016](#)) based representation learning. Projection Networks project the 3D point cloud onto 2D image planes from multiple viewpoints and use 2D Convolutional Neural Networks (2D-CNN) ([Goodfellow et al., 2016](#)) to process them ([Su et al., 2015](#)), ([Boulch et al., 2017](#)), ([Lawin et al., 2017](#)). Voxel-based methods project the point cloud onto a 3D grid ([Maturana & Scherer, 2015](#)), ([Roynard et al., 2018](#)), ([Ben-Shabat et al., 2018](#)). Sparse data structures like octree and hash-maps are used for better efficiency and larger context sizes ([Graham et al., 2018](#), [Riegler et al., 2017](#)). These grids are further processed using 3D Convolutional Neural Networks (3D-CNN) ([Goodfellow et al., 2016](#)). The main drawbacks of these approaches arise from the loss of details in the original point cloud structure during projection onto grids ([Thomas et al., 2019](#)). Graph Convolutional Networks address this problem by retaining the original position of each point and combining features on local surface

patches (Verma et al., 2018, Wang et al., 2019). However, their representation is invariant to the deformations of those patches in Euclidean space which is not helpful for estimating non-rigid transformations between point clouds (Thomas et al., 2019). Pointwise Networks like PointNet (Qi et al., 2017) apply a shared neural network to each point followed by global max-pooling. This approach set new benchmarks in point-cloud classification and different variants using Multi-Layer Perceptron (MLP) (Qi et al., 2017), (Li et al., 2018, Liu et al., 2019) and CNN (Atzmon et al., 2018, Groh et al., 2018, Hua et al., 2018, Xu et al., 2018).

Kernel Point Convolution (KPConv) (Thomas et al., 2019) is one of the recent breakthroughs in point cloud representation learning and is particularly suitable for deformable point clouds. Figure 2.1 illustrates the procedure. It learns a kernel function to compute pointwise filters and increases representation power using deformable kernels. Instead of a grid-shaped kernel (as is the case with regular 2D and 3D CNNs), the kernel points in KPConv are spread freely in space. Each kernel point accumulates the features of the point-cloud points within a spherical neighborhood around itself with weights that decay as the points get farther. In deformable KPConv, each kernel point also has a learnable offset that allows it to learn to adapt the shape of a kernel to different inputs. We will use KPConv to learn representations of our point clouds in the experiments for this thesis.

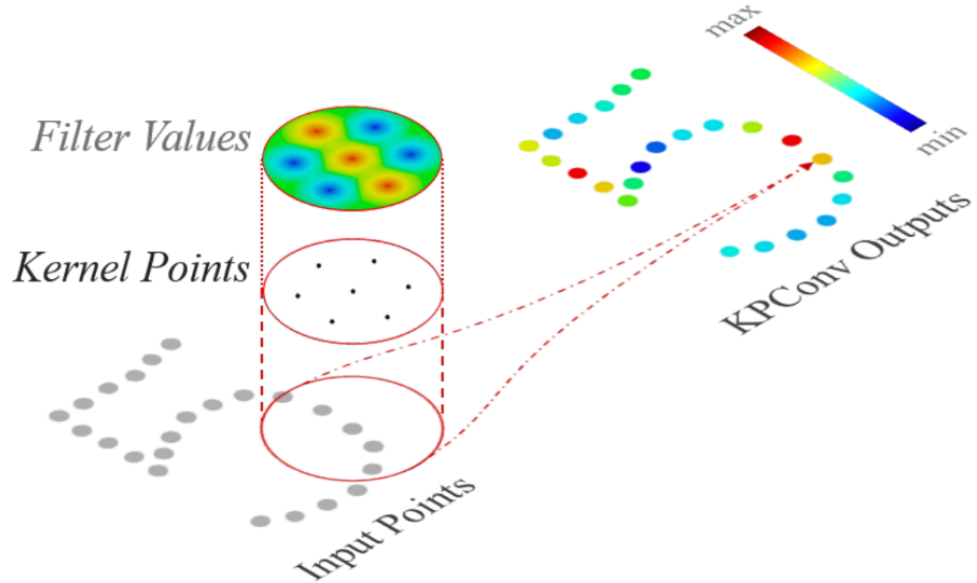


FIGURE 2.1: Kernel Point Convolution (Thomas et al., 2019) (KPConv) demonstrated on 2D points.

2.2.2 Feature matching and registration

After the points have been represented using feature vectors, the next task is to find corresponding points between the given pair of point clouds.

2.2.2.1 Rigid Registration

Traditional methods use different variants of the RANdom SAMple Consensus (RANSAC) algorithm for finding matching points (Holz et al., 2015, Schnabel et al., 2007). RANSAC is an iterative algorithm and works by classifying all possible correspondences into inliers and outliers. RANSAC is simple yet powerful and a bulk of the literature on point cloud registration uses RANSAC with both handcrafted and learned features (Ao et al., 2021), (Bai et al., 2020), (Choy et al., 2019), (Deng et al., 2018a), (Deng et al., 2018b), (El Banani et al., 2021), (Yu et al., 2021), (Zeng et al., 2017). For rigid point clouds, another popular algorithm is Iterative Closest Point (ICP) (Arun et al., 1987), (Besl & McKay, 1992), (Zhang, 1994). ICP assumes that the two point clouds are spatially close. In each iteration, for each point in the source point cloud, the closest point in the destination cloud is assigned as the matching point. Then the rigid transformation (rotation and translation) is computed by minimizing mean-square loss. These steps are repeated till convergence. Direct Registration approaches combine feature extraction, feature matching, and registration within a single architecture through end-to-end pose optimization (Besl & McKay, 1992), (Zhou et al., 2016), (Aoki et al., 2019), (Choy et al., 2020).

2.2.2.2 Non-rigid registration

Non-rigid correspondence has the added challenge of accounting for deformations. Different approaches have been proposed including projective correspondence (Newcombe et al., 2015), Siamese Network (Schmidt et al., 2016), and Scene Flow estimation (Li et al., 2021), (Liu et al., 2019), (Puy et al., 2020). Non-rigid correspondence is also studied in Geometry Processing where the input data is in the form of manifold surfaces. Methods like isometric deformation (Huang et al., 2008), latent code optimization (Groueix et al., 2018), and functional maps (Ovsjanikov et al., 2012) have been studied in this context.

2.2.3 Challenges

Real-world applications of point cloud registration are faced with several challenges. We discuss these in this section.

2.2.3.1 Lack of ordering or structure

A point cloud is a collection of points in 3D space with no ordering or structure (like a grid). The absence of a grid structure makes it difficult to apply traditional deep learning methods like CNNs because they leverage the grid structure of their inputs (images/videos) for learning representations. As described in the previous section, there have been attempts (Ben-Shabat et al., 2018, Lawin et al., 2017, Maturana & Scherer, 2015, Roynard et al., 2018), to coerce/quantize/project point clouds to grids in order to harness the power of traditional CNNs while trading off the loss of the inherent structural details of the point cloud. New forms of convolution like KPConv (Thomas et al., 2019) also attempt to address this challenge with flexible non-grid kernels.

2.2.3.2 Sparsity

Most real-world 3D scans tend to be sparse 2.2. As a result of this, a large amount of computing gets wasted processing zero entries. For efficient processing of sparse point clouds using Deep Neural Networks, the recently proposed Minkowski Engine (Choy et al., 2019) has proved to be a game changer. It represents point clouds as a position-indexed array and performs computation only for invalid regions. It can also leverage specialist hardware like GPU for greater throughput.

2.2.3.3 Noise and Outliers

Real-world 3D scans can be dirty with a large amount of noise and outliers 2.3. These are points that do not belong to the intended surface. One of the sources of outliers is a specular reflection from shiny surfaces like metal. In rigid registration, the RANSAC algorithm (Holz et al., 2015, Schnabel et al., 2007) attempts to remove the outliers that do not conform with the model with maximum consensus. Learning approaches to outlier detection and removal include (Bai et al., 2021, Pais et al., 2020).

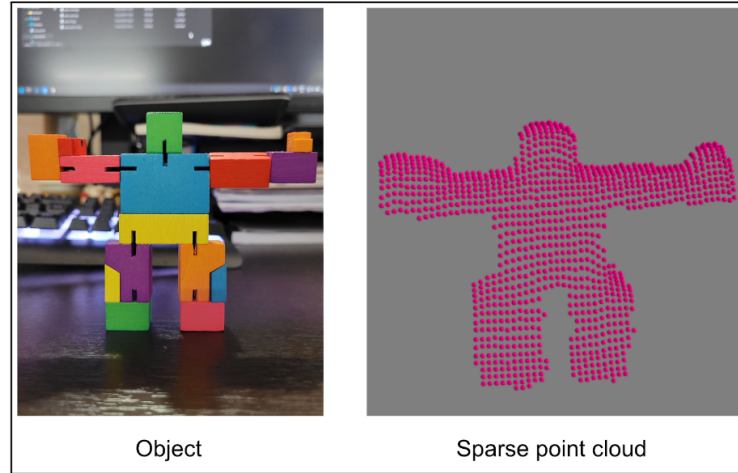


FIGURE 2.2: Example of sparse point cloud scan



FIGURE 2.3: Example of noise in point clouds scanned by Microsoft HoloLens 2.

2.2.3.4 Partial Overlap

In a real-world use case of point cloud registration, the source and target point clouds may only have a partial match [2.4](#) albeit the fact that they are of the same object. This might be due to occlusion, object motion, or viewpoint change. A variety of methods have been proposed to perform the registration of point clouds that have a partial match ([Attaiki et al., 2021](#), [Rodolà et al., 2017](#), [Thomas et al., 2019](#), [Xu et al., 2021](#)).

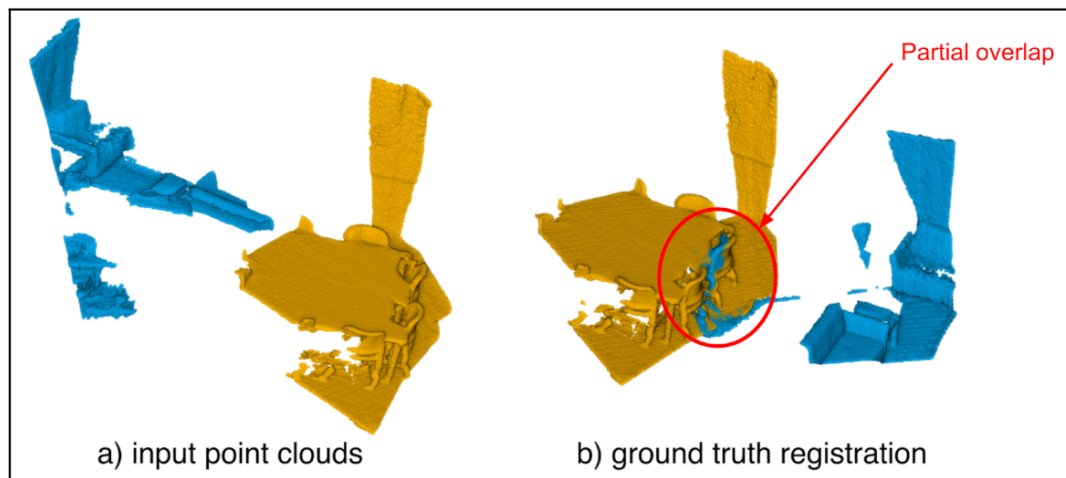


FIGURE 2.4: Example of partial overlap between the source and target point clouds

2.3 Conclusion

In this chapter, we presented a review of point cloud registration algorithms. We presented the challenges of point cloud registrations that arise from real world use cases. This section serves to provide a background for the studies that we present in the following chapters of the thesis.

Chapter 3

Research Methodology

3.1 Introduction

In this chapter, we present our research methodology. We describe the datasets used for training the neural network models used in our experiments. We also present the details of our real world evaluation setup. We use different point cloud registration metrics to evaluate the proposed algorithms. These are also described in this chapter.

3.2 Research Tools

First, we discuss our research tools. Our research tools include specialised hardware and software.

3.2.1 Hardware

The hardware required in this project can be categorized into three categories:

- Data capture devices,
- Data processing devices, and
- Data rendering devices.

3.2.1.1 Data capture devices

For the capture of 3D data, we use Microsoft HoloLens 2 (Ungureanu et al., 2020). As shown in Figure 1.1, Hololens 2 comes with a 1-MP time-of-flight based depth sensor for scanning point clouds and an 8-MP RGB camera for capturing textures. The depth camera has short and long throw modes for capturing points at different distances from the user. In addition to this, it has 4 visible light cameras for head tracking. This produces posed point clouds. The availability of camera pose makes it possible to register multiple scans of the same object from different angles and reduce holes and noise in the scan.

3.2.1.2 Data processing devices

For computation, we use two high-performance laptop computers with one GPU each. The following are the details:

- 2020 Lenovo Legion with RTX-2080 GPU. This GPU comes with 8-GB GDDR6 memory.
- 2016 Asus Republic Of Gamers with GTX-1080 GPU. This GPU comes with 8-GB GDDR5X memory.

Large point clouds can be tricky to fit along with large neural network models within the limited GPU memory. As explained in Section 6.2.3, we may need to downsample point clouds before feeding them into the registration pipeline. This creates a trade-off between the use of high-performance neural networks that are heavy on GPU memory and the level of detail in the input point clouds.

3.2.1.3 Data rendering devices

For rendering the results of registration, we use the same Microsoft Hololens 2. The source CAD model is assumed to be located at the origin of the Hololens frame coordinates. However, during the computation of transformations for registration, we use world coordinates for both the source and target point clouds. The mapping from Hololens frame coordinates and world coordinates is obtained

through Simultaneous Localization And Mapping (SLAM) (Durrant-Whyte & Bailey, 2006). After the transformations for registration have been obtained in the world coordinate system, they are converted into the Hololens’ current frame coordinates. These transformations are then applied to the source model and the transformed model is rendered.

3.2.2 Software

Our registration codebase is a fork of our open-source baseline, Leopard [(Li & Harada, 2022)]. The code is written mostly in Python. We use HoloLens 2 Research Mode (Ungureanu et al., 2020) for processing the raw scans from the MR platform and extracting and processing point clouds. For visualisation, we use Unity (Jerald et al., 2014), CloudCompare (Girardeau-Montaut, 2016) and Meshlab (Cignoni et al., 2011).

3.3 Datasets for our Study

We will consider training and fine-tuning our models on the following datasets.

- 3DMatch (Zeng et al., 2017) and 3DLoMatch (Li et al., 2021): These are datasets for rigid-body partial point cloud registration consisting of indoor scans. “Lo” in the name 3DLoMatch denotes the low level of overlap between the source and target point clouds. 3D Match is a collection of 62 scenes which are mostly scans of indoor environments. The official 3DMatch dataset only contains those examples that have more than 30 percent overlap between the source and target point clouds. 3DLoMatch is its counterpart that contains the scan pairs with 10-30 percent overlap.
- 4DMatch and 4DLoMatch (Li & Harada, 2022): These are datasets for non-rigid partial point cloud registration derived from DeformingObjects4d (Li et al., 2021), a dataset of animated characters. “Lo” in the name 4DLoMatch denotes the low level of overlap between the source and target point clouds in the test set. The DeformingObjects4d dataset has 1972 animation sequences with dense ground-truth correspondences between points. The 4DMatch dataset consists of a randomly selected subset of 1761 animation sequences

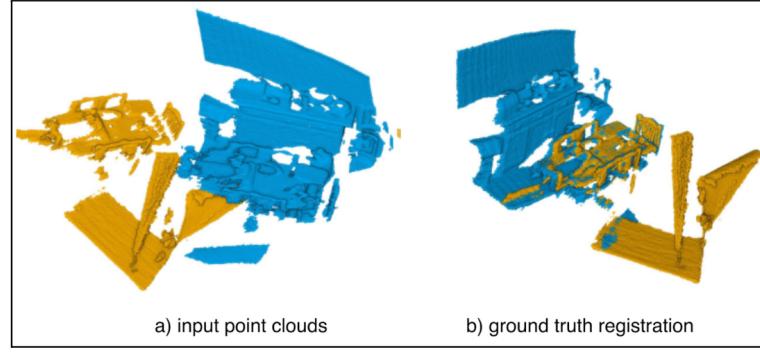


FIGURE 3.1: Kernel Sample data point from 3DMatch dataset.

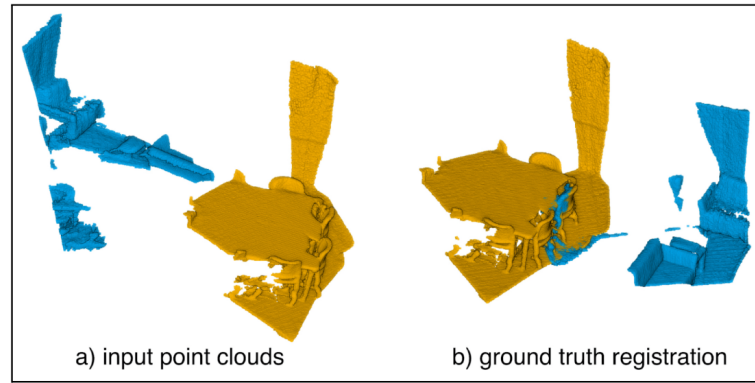


FIGURE 3.2: Sample data point from 3DLoMatch dataset.

from DeformingObjects4d. The training, validation and test splits of this dataset are of sizes 1232, 176 and 353 respectively. The 4DLoMatch dataset has the same training and validation splits as the 4DMatch dataset. The 353 test samples are distributed between 4DMatch and 4DLoMatch as follows: 4DLoMatch has all the samples that have an overlap ratio between the source and target point clouds of less than 45 percent. If the overlap ratio is 45 percent or higher, the sample is assigned to 4DMatch. Figure 8 shows a few examples from these datasets.

4DMatch and 4DLoMatch (Li & Harada, 2022) are composed of animated objects. However, for real-world use cases in Mixed Reality, Robotics, etc. we must evaluate the performance of non-rigid registration on noisy scans of real deformable objects. We collect such data with our Microsoft HoloLens 2 MR device and Azure Kinect RGB-D camera. Figure 9 shows some test objects that we plan to use for evaluation in this project. Figures 10 and 11 show our test environment that is cluttered and represents a typical real-world usage environment of Mixed Reality devices.

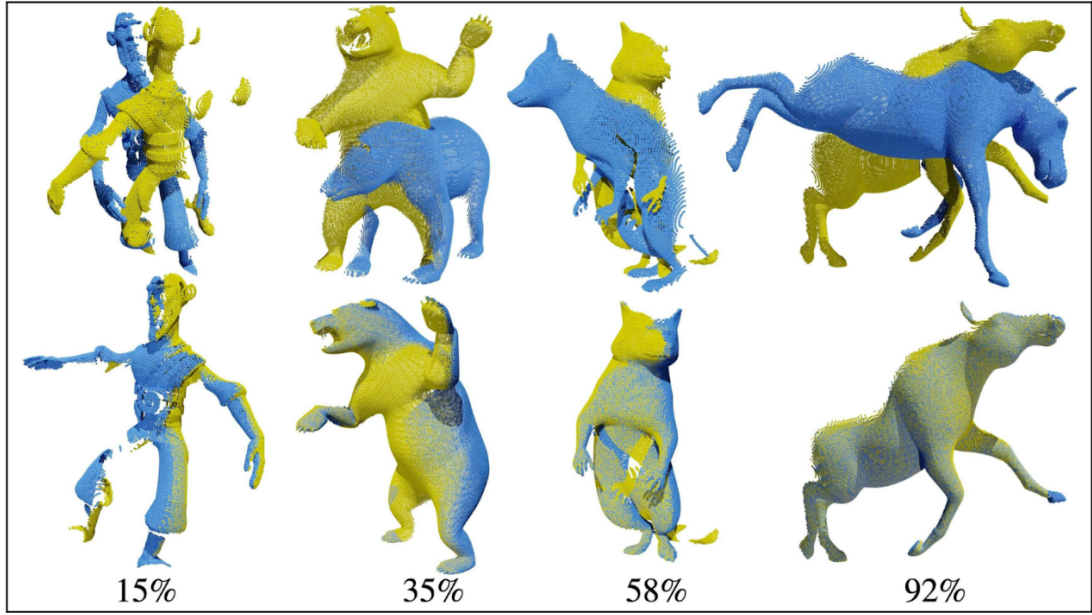


FIGURE 3.3: Samples from the 4DMatch/4DLoMatch dataset. The top row shows the input source and target point clouds and the bottom row shows the ground truth registration outcomes. The percentages at the bottom of the figure denote the percentage of overlap between the source and target point clouds in each of these examples.

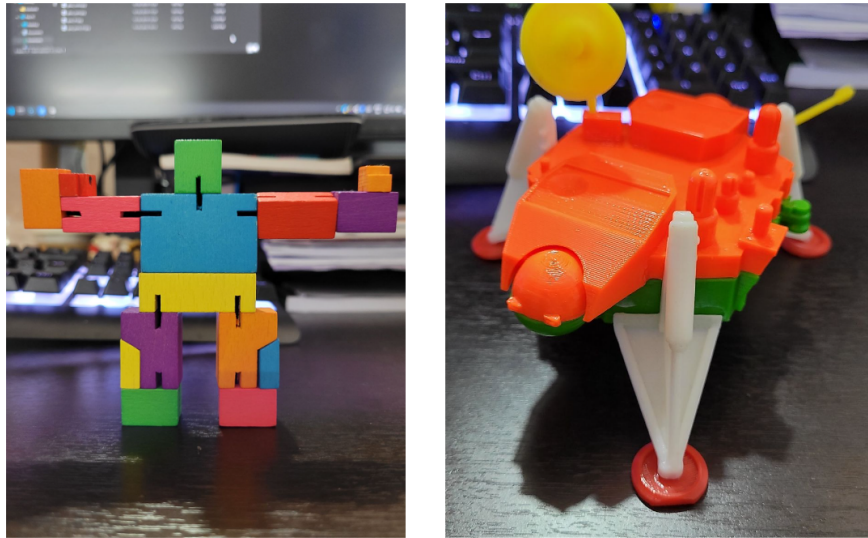


FIGURE 3.4: Real-world objects used for our study. (Left) Cubebot robot model (non-rigid). (Right) NASA Lander model (rigid)

3.4 Data Visualisation

Visualization is extremely necessary for debugging and analyzing point cloud registration results. We use several tools for visualization. For debugging purposes,



FIGURE 3.5: Real-world environment (cluttered) used in our tests.

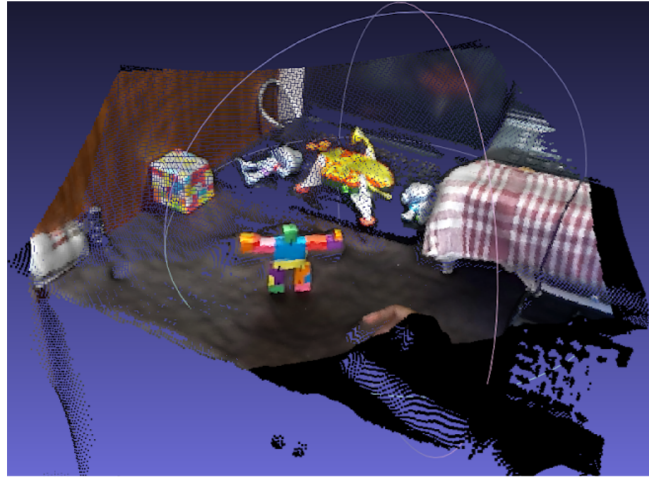


FIGURE 3.6: Point cloud scan of the real-world cluttered test environment.
Scan generated using Microsoft HoloLens 2.

we use Matplotlib ([Hunter, 2007](#)), Open3D [Zhou et al. \(2018\)](#), and Mayavi ([Ramachandran & Varoquaux, 2011](#)) Python libraries within our workflow. For a detailed analysis of registration results, we use Cloud Compare ([Girardeau-Montaut, 2016](#)) and MeshLab ([Cignoni et al., 2011](#)).

3.5 Training Objectives

The following are the loss functions used to train Lepard ([Li & Harada, 2022](#)):

- **Matching Loss:** The Focal Loss over the confidence matrix returned by the matching layer is minimised.

- **Warping Loss:** This is the L1 Loss between the target point cloud and the source point cloud warped by the Rotation and Translation matrices returned by the Procrustes layer.

3.6 Evaluation Metrics

The following are the metrics used for benchmarking point cloud registration algorithms:

- **Inlier ratio (IR).** The inlier Ratio is the fraction of correct matches in the predicted correspondences set.

$$IR = \frac{1}{|\mathcal{K}_{pred}|} \sum_{(\mathbf{p}, \mathbf{q}) \in \mathcal{K}_{pred}} \left[\|\mathcal{W}_{gt}(\mathbf{p}) - \mathbf{q}\|_2 < \sigma \right]$$

The diagram includes the following callouts:

- Set of predicted correspondences:** A yellow callout pointing to $|\mathcal{K}_{pred}|$.
- Ground truth warp function:** A green callout pointing to \mathcal{W}_{gt} .
- L2-norm:** A cyan callout pointing to $\|\cdot\|_2$.
- Iverson bracket:** A red callout pointing to the entire expression in the brackets $[\cdot]$.

FIGURE 3.7: Illustration of the Inlier Ratio (IR) metric.

- **Non-rigid Feature Matching Recall (NFMR).** NFMR measures the fraction of ground-truth matches that were successfully recovered by the correspondence prediction algorithm.

3.7 Baseline Selection

We choose Leopard (Li & Harada, 2022) as our baseline algorithm as it is one of the current state-of-the-art methods for partial non-rigid point cloud registration. The algorithm uses powerful KPConv [(Thomas et al., 2019)] for learning deformable point cloud representations. In order to add positional information to the translation invariant KPConv representation, the authors use Rotary Positional Encoding

$$\text{NFMR} = \frac{1}{|\mathcal{K}_{gt}|} \sum_{(\mathbf{u}, \mathbf{v}) \in \mathcal{K}_{gt}} [\|\Gamma(\mathbf{u}, \mathcal{A}, \mathcal{F}) - \mathbf{v}\|_2 < \sigma]$$

where

$$\Gamma(\mathbf{u}, \mathcal{A}, \mathcal{F}) = \sum_{\mathcal{A}_i \in \text{knn}(\mathbf{u}, \mathcal{A})} \frac{\mathcal{F}_i \|\mathbf{p} - \mathcal{A}_i\|_2^{-1}}{\sum_{\mathcal{A}_i \in \text{knn}(\mathbf{u}, \mathcal{A})} \|\mathbf{u} - \mathcal{A}_i\|_2^{-1}}$$

Ground Truth correspondences

K-nearest neighbors

Anchor points

FIGURE 3.8: Illustration of the Non-rigid Feature Matching Recall (NFMR) metric

[93]. For point cloud matching it uses the RANSAC algorithm [(Holz et al., 2015)] for rigid objects and deformable ICP for non-rigid objects. A transformer is used for position-aware feature matching and Rigid Fitting with Soft Procrustes [(Besl & McKay, 1992)] is used to obtain the final Rotation and Translation values for the transformation/warp function.

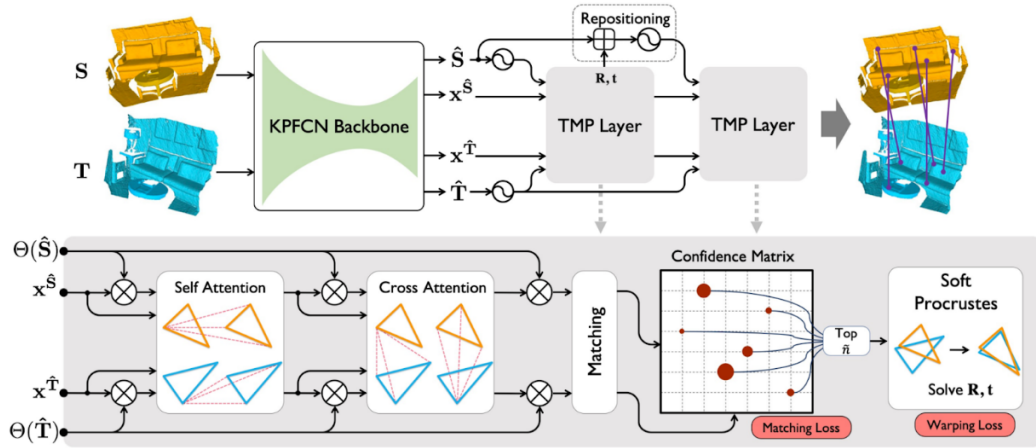


FIGURE 3.9: Flowchart depicting the architecture of Lepard. Please refer to the paper (Li & Harada, 2022) for details.

3.8 Conclusion

In this chapter, we described our research methodology. We provided key details about the datasets used for training and real world evaluation. Mixed reality is a compute intensive field. So we also disclosed the hardware available for our study. We described our baselines and explained the evaluation metrics.

Chapter 4

Non-Rigid Point Cloud Registration

In this chapter, we present a detailed account of the non-rigid point cloud registration workflow adopted in this research project. Our workflow is based on Lepard ([Li & Harada, 2022](#)) and Iterative Closest Point (ICP) algorithms ([Arun et al., 1987](#), [Besl & McKay, 1992](#), [Zhang, 1994](#)) that we discuss in details in this chapter. This will serve as a prelude to the novel methods that we present in the next chapter of the thesis.

4.1 Introduction

We adopt a modular workflow similar to Lepard ([Li & Harada, 2022](#)). Modular workflows are more interpretable and easily upgradable than end-to-end workflows ([Glasmachers, 2017](#)). There are three main steps in this workflow:

1. Finding correspondences between “feature points” in the source and target point clouds.
2. Whole body “Rigid fitting” using the correspondences discovered.
3. Non-rigid registration to warp the surface of the source point cloud onto the target.

The most challenging task in the entire workflow is finding the correspondences in the presence of arbitrary deformations, occlusions, and holes. Lepard (Li & Harada, 2022) is a state-of-the-art algorithm for finding non-rigid correspondences. We use the same in our pipeline. Lepard provides two options to accomplish the second step - RANSAC (Holz et al., 2015, Schnabel et al., 2007) and soft-prucrustes (Arun et al., 1987). It is important to note that non-rigid deformations are applied to the source point cloud only at the final step. The authors of Lepard leveraged the Non-rigid Iterative Closest Point algorithm (Li et al., 2008, Zollhöfer et al., 2014) for finding a rigid transformation for each point on a mesh representation of the surface of the source point cloud. We discuss these components in detail in this section.

4.2 Lepard: Learning partial point cloud matching in rigid and deformable scenes

Lepard is a point cloud matching algorithm that has been shown to be effective even when the source and target point clouds are noisy, and incomplete and the degree of overlap is low. It addresses the challenge of disambiguation between repetitive geometry patterns - for example, the two hands of a human, and multiple instances of identical chairs in a room. Prior methods used the geometry features extracted by 3D Convolutional Neural Networks (3D-CNNs) (Singh et al., 2019) that are designed to be translation invariant like other Convolutional Neural Networks. These representations also tend to be rotation invariant due to the use of max-pooling layers in the network and data augmentation using random rotations of the same input during training. The authors observe that rotation and transformation invariant features can cause repetitive geometry patterns to be assigned identical representations. So left and right hands of the same person would look the same after embedding. All the chairs of the same kind in the scene would also be difficult to distinguish in the embedding space. Motivated by the tendency of humans to associate things not just their appearance but also by their relative positions, the authors propose to enhance the 3D geometry representations with 3D positional information to help with disambiguation.

4.2.1 Notation

We use the same notation as the authors of Lepard in our paper. Let $\mathbf{S} \in \mathbb{R}^{n \times 3}$ be the source point cloud (with n points) and $\mathbf{T} \in \mathbb{R}^{m \times 3}$ be the target point cloud (with m points). Our goal is to calculate a warp function $\mathcal{W} : \mathbb{R} \rightarrow \mathbb{R}$ that maps \mathbf{S} to \mathbf{T} . For an arbitrary non-rigid deformation, \mathcal{W} generalizes to a dense per-point warp field. For the rigid case, \mathcal{W} can be parameterized as a $SE(3)$ transformation which is a single rotation and a single transformation applied to the whole body of \mathbf{S} .

4.2.2 Local geometry feature extraction

Lepard uses Kernel Point Convolution (Thomas et al., 2019) based on a Fully Convolutional Neural Network (KPFCN) for representation learning. The KPFCN backbone uniformly downsamples both \mathbf{S} and \mathbf{T} for efficient computation. This is particularly crucial for the transformer and matching modules that come next. Both of them have $\mathcal{O}(n^2)$ time complexity. Again, following the notation used by the authors of Lepard, we denote the downsampled source and target point clouds by $\hat{\mathbf{S}}$ and $\hat{\mathbf{T}}$ respectively. These go as input to the KPFCN network for feature extraction. We discuss KPFCN next.

4.2.2.1 Kernel Point Convolution

The remarkable progress of image recognition algorithms in the past decade has been fuelled in a large part by Convolutional Neural Networks (CNNs) (Rawat & Wang, 2017). These networks leverage the grid structure of 2D images for high comput efficiency on modern hardware like GPUs. Inspired by this success, many 3D convolutional network based algorithms were proposed for processing point cloud scans. However, point clouds do not come in a 3D grid structure. Hence 3D-CNN methods had to synthetically put the points in a regular grid structure resulting in the loss of critical structural information. This was particularly amplified in the case of sparse clouds and varying density. The authors of Kernel Point Convolution (KPConv) (Thomas et al., 2019) were motivated by the need to work around the grid assumption and proposed a flexible, deformable convolution operator that retains the original structure of the point cloud (spatial localization).

We formally introduce KPConv using notation from the paper (Thomas et al., 2019). Let us consider a point cloud $\mathbf{P} \in \mathbb{R}^{n \times 3}$ with point features $\mathcal{F} \in \mathbb{R}^{n \times D}$. Let $f_i \in \mathcal{F}$ denote the feature vector representing point $x_i \in \mathbf{P}$. KPConv consists of a set of local 3D filters. For a kernel g , the normal convolution operation works as shown in Equation 4.1.

$$(\mathcal{F} * g)(x) = \sum_{x_i \in \mathcal{N}(x)} g(x_i - x) f_i \quad (4.1)$$

Where $\mathcal{N}(x)$ denotes a neighborhood of the point x , a region where the kernel g is applied. The authors note that a spherical neighborhood is more effective against varying density than a K-nearest neighbor (KNN) neighborhood. So, $\mathcal{N}(x) = \{x_i \in \mathbf{P} \mid \|x_i - x\| \leq r\}$ where $r \in \mathbb{R}$ is the radius of the neighborhood. The authors call this neighborhood $\mathcal{N}(x)$ centered at x , the domain of definition of kernel g . All points in \mathbf{P} that lie within this domain of definition will be influenced by g . However, we would like to have different amounts of influence on different points depending on their distance from x . Writing relative distance from x as $y_i = x_i - x$, we have the domain of definition of g as $\mathcal{B}_r^3 = \{y \in \mathbb{R}^3 \mid \|y\| \leq r\}$. Each kernel g has K kernel points $\{\tilde{x}_k\}_{k=0}^{K-1} \subset \mathcal{B}_r^3$. Each kernel point \tilde{x}_k is assigned a weight $W_k \in \mathbb{R}^{D \times D_{out}}$. For any point $y \in \mathcal{B}_r^3$ the kernel function g is defined as in equation 4.2.

$$g(y) = \sum_{k=0}^{K-1} h(y, \tilde{x}_k) W_k \quad (4.2)$$

Here h is the correlation between the features of the point y and the kernel point \tilde{x}_k . Points closer to \tilde{x}_k will likely have a higher correlation with \tilde{x}_k and hence will be influenced more by the corresponding weight W_k . The authors compute the correlation function using the linear formulation in equation 4.3.

$$h(y, \tilde{x}_k) = \max \left(0, 1 - \frac{\|y - \tilde{x}_k\|}{\sigma} \right) \quad (4.3)$$

KPConv comes in two variants - rigid and deformable. In rigid KPConv, the kernel points are fixed. In deformable KPConv, the kernel points have learnable offset parameters $\Delta_k(x)$. Deformable KPConv is able to adjust the shape of the kernel and adapt the kernel points to the local geometry.

4.2.3 Relative 3D Positional Encoding

Representations learned by the KPFCN backbone are translation and rotation invariant due to reasons discussed before. In order to disambiguate between repetitive geometry features, the authors of Lepard propose to enhance the KPFCN features using 3D positional encoding.

The most popular kind of positional encoding method is sinusoidal positional encoding (Vaswani et al., 2017). A set of M discrete sinusoids and co-sinusoids at different frequencies are defined over the size of the input space and these are sampled at each point x to obtain a $2M$ dimensional encoding that reflects the relative position of the point. The authors of Lepard chose to use the Rotary Positional Encoding scheme of the Roformer paper (Su et al., 2021). Given a 3D point $S_i \in \mathbb{R}^3$ with feature vector $x_i^S \in \mathbb{R}^D$, the positional encoding function is defined as in equation 4.4.

$$PE(S_i, x_i^S) = \Theta(S_i)x_i^S \quad (4.4)$$

Where $\Theta(S_i)$ is a block diagonal matrix.

The authors argue that it is a better choice than sinusoidal in the case of point clouds because:

1. The embedding only changes the feature's direction, not the feature's length. This can potentially improve the stability of training.
2. The dot product of two spherical embedding feature vectors explicitly reveal the Euclidean distance between the corresponding points as demonstrated in equation 4.5.

$$PE(S_i, x_i^S)^T PE(S_j, x_j^S) = [\Theta(S_i)x_i^S]^T \Theta(S_j)x_j^S = (x_i^S)^T \Theta(S_j - S_i)x_j^S \quad (4.5)$$

In the last step $\Theta(S_i)^T \Theta(S_j) = \Theta(S_j - S_i)$ is a result of the construction of the matrix Θ .

4.2.4 Transformer

Let us represent the outcome of local geometry feature extraction as $x^{\hat{S}}$ and $x^{\hat{T}}$ for the source and target point clouds respectively. Lepard uses a transformer network to compute the self attention within the points of the same cloud and cross attention between the points in the source and target clouds. While self-attention collects global context, cross attention helps in the exchange of information between the source and target clouds.

Attention mechanism works by computing query (\mathbf{q}), key (\mathbf{k}) and value (\mathbf{v}) vectors using learnable projection matrices W_q , W_k and W_v for each point in the point cloud as follows:

$$\begin{aligned} q_i &= \Theta(\hat{S}_i)W_q x_i^{\hat{S}} \\ k_i &= \Theta(\hat{S}_i)W_k x_i^{\hat{S}} \\ v_i &= W_v x_i^{\hat{S}} \end{aligned} \tag{4.6}$$

4.2.4.1 Self Attention Layer

In the self attention layer, the features of each point are updated as in equation

$$x_i^{\hat{S}} = x_i^{\hat{S}} + MLP(\text{cat}[q_i, \sum_j a_{ij} v_j]) \tag{4.7}$$

where $a_{ij} = \text{softmax}(q_i k_j^T / \sqrt{D})$ is the attention weight, MLP is a 3-layer multi-layer perceptron and cat is the concatenation operator.

4.2.4.2 Cross Attention Layer

The mathematical construct of the cross attention layer is identical to the self attention layer. The only difference is that the query q and the key-value pair (k, v) come from different point clouds. Lepard computes cross attention both ways: $\hat{S} \rightarrow \hat{T}$ and $\hat{T} \rightarrow \hat{S}$.

4.2.5 Position-aware Feature Matching

The transformer layer is followed by feature matching. The scoring matrix \mathcal{S} between the source and target point clouds is computed as in equation 4.8.

$$S(i, j) = \frac{1}{\sqrt{D}} \langle \Theta(\hat{S}_i) W_{\hat{S}} x_i^{\hat{S}}, \Theta(\hat{T}_j) W_{\hat{T}} x_j^{\hat{T}} \rangle \quad (4.8)$$

Here, \langle, \rangle denotes inner product. $W_{\hat{S}}, W_{\hat{T}} \in \mathbb{R}^{D \times D}$ are learnable projection matrices. The use of point representations with positional encoding makes sure that the matching algorithm takes spatial distance into account. The scoring matrix is converted into a confidence matrix \mathcal{C} using a dual-softmax operation as shown in equation 4.9.

$$\mathcal{C}(i, j) = \text{Softmax}(\mathcal{S}(i, \cdot)) \cdot \text{Softmax}(\mathcal{S}(\cdot, j)) \quad (4.9)$$

The confidence scores are thresholded at a given minimum value θ_c to determine matches. θ_c is a hyperparameter.

4.2.6 Rigid Fitting with Soft Prucrustes

Once the correspondence matches between the points in \hat{S} and \hat{T} have been found, a rigid transformation (consisting of a rotation matrix $R \in SO(3)$ and a translation vector $t \in \mathbb{R}^3$) is derived to fit this correspondence as closely as possible. This process is known as rigid fitting with Soft Prucrustes (Arun et al., 1987). From the correspondence matrix \mathcal{C} , the top \hat{n} scoring matches are chosen. Let us call this set \mathcal{K}_{soft} . The next step is to construct the matrix \mathcal{H} as in equation 4.10.

$$H = \sum_{(i,j) \in \mathcal{K}_{soft}} \tilde{C}(i, j) \hat{S}_i \hat{T}_j^T \quad (4.10)$$

$\tilde{C}(i, j)$ is the normalized confidence score. Next, rotation R is computed as in equation 4.11.

$$R = U \text{diag}(1, 1, \det(UV^T)) V \quad (4.11)$$

U and V are obtained from an SVD decomposition of $H = U\Sigma V^T$. The translation t is obtained as in equation 4.12.

$$t = \frac{1}{|\mathcal{K}_{soft}|} \left(\sum_{(i,\cdot) \in \mathcal{K}_{soft}} \hat{S}_i - R \sum_{(\cdot,j) \in \mathcal{K}_{soft}} \hat{T}_j \right) \quad (4.12)$$

4.3 Non-rigid Registration

After rigid fitting with the R and t matrices derived in the previous section, non-rigid registration is performed for warping the surface of the source point cloud on to the target. Non-rigid Iterative Closest Point (N-ICP) algorithm (Li et al., 2008, 2021) is one of the common approaches to this. There are two categories of registration algorithms:

- **Dense registration:** Dense registration methods find a mapping from each point in the template on to the target.
- **Sparse registration:** Sparse registration methods find correspondences only for selected feature points.

N-ICP is a dense registration algorithm.

4.3.1 Non-rigid Iterative Closest Point (N-ICP)

Registering two surfaces means finding a mapping between a template surface and a target surface that describes the position of semantically corresponding points. This is also known as warping the template onto the target. The task of a registration algorithm is to choose the correct deformation from all possible warps by imposing constraints on the deformation. This is known as “regularisation of the deformation field”.

N-ICP(Li et al., 2008, 2021) applies a locally affine regularisation that assigns an affine transformation to each vertex and minimises the difference in the transformation of neighbouring vertices. With this regularisation, the optimal deformation for fixed correspondences and fixed stiffness can be determined exactly and

efficiently. The algorithm loops over a series of decreasing stiffness weights that results in incremental deformation of the template surface towards the target. In order to determine the optimal deformation for a given stiffness:

1. Preliminary correspondences are estimated by a nearest point search.
2. The optimal deformation of the template for these fixed correspondences and the active stiffness is then calculated.
3. Go to Step 1 to find new correspondences by searching from the displaced template vertices.

In the ideal case, for noiseless and complete data, the correct registration should have a one-to-one correspondence. But in practice, the surfaces contain holes and artefacts resulting from the scanning process. A useful registration method needs to be robust against outliers and must fill in missing data in a sensible way. Missing data needs to be filled in using knowledge from the template mesh. N-ICP achieves this by smoothly deforming the template mesh.

4.4 Conclusion

In this chapter, we described key non-rigid registration algorithms that are used in our pipeline. We presented Lepard (Li & Harada, 2022) for non-rigid correspondence matching and N-ICP for non-rigid registration. We also pointed out the challenges involved in applying these methods in a real world mixed reality application and motivated the methods proposed in the following chapter for the use case of our focus.

Chapter 5

Proposed Method

5.1 Introduction

In the previous chapter, we discussed the non-rigid point cloud registration workflow. We discussed how Lepard ([Li & Harada, 2022](#)) provides an effective method of finding correspondences between point clouds undergoing non-rigid deformations. We also discussed how correspondence matching step is followed by a non-rigid registration step where methods like N-ICP ([Holz et al., 2015](#), [Schnabel et al., 2007](#)) are used to warp a mesh representation of the source point cloud on to the target point cloud taking into account noise, holes and missing parts. Our contributions in the thesis are restricted to the non-rigid registration step and they are tailor-made for an important task in Mixed Reality applications which we discuss in this chapter.

5.2 Motivation

In N-PCR algorithms like Lepard, after rigid fitting, dense registration methods like N-ICP ([Li et al., 2008, 2021](#)) are used to optimally morph the source mesh on the surface of the target point cloud. This involves finding a transformation for each point on the source mesh and the computational requirement can blow up for large meshes.

In this work we want to focus on the problem of registration of CAD models to 3D scans of rigid objects with rigid movable parts. Some examples are machine

parts with hinges and appliances with movable antennas. As we manipulate such objects, the movable parts may move relative to the object resulting in a non-rigid deformation. Most applications of non-rigid registration in enterprise mixed reality involve such objects.

For the objects of interest, we can safely assume that the parts do not deform within themselves. Under this assumption, the non-rigid adjustment step after rigid fitting boils down to finding a rigid transformation for each part that can move relative to one another.

5.3 Challenges

There are several challenges in the proposed approach.

1. The first is to make sure that the object model does not disintegrate after applying part-wise registration.
2. The second challenge is to search for a given part in the right part of the target point cloud.
3. The third challenge is to take into consideration the presence of outliers. For small parts, outliers can have a large impact on the predicted correspondences.

5.4 Our approach

In this section, we discuss our proposed algorithm for non-rigid registration of rigid objects with rigid moving parts. We present our psuedocode of our proposed method in Algorithm 1. We explain our algorithm with an example registration task on a model of the NASA Lunar Lander¹ shown in Figure 5.1. The source and target point clouds are shown in figure 5.2. In addition to a whole body rigid translation and rotation, the deformable parts *dish*, *dish-pole*, *sensor*, *sensor-pole*, *sensor-joint* and *antenna* have moved relative to the static components of the model in the target point cloud. The algorithm proceeds as explained below.

¹Open source model of NASA Viking Lander obtained from <https://nasa3d.arc.nasa.gov/detail/viking-lander>

Algorithm 1 Pseudocode of part-whole registration.

Input: Source point cloud \mathbf{S} with its parts $\{p_i^S\}_{i=1}^{n_{parts}^S}$ labelled; Target point cloud \mathbf{T} ; Retention fraction $f_{retention}^{subsample}$ for point-cloud subsampling; Maximum correspondence distance d_{max}^{corr} for ICP; Minimum number of correspondences n_{min}^{corr} for RANSAC.

Output: A rigid transformation (R_i, t_i) for each part p_i^S in the source point cloud.

- 1: Ingest S and T and subsample them, retaining $f_{retention}^{subsample}$ fraction of the samples in order to fit in the GPU memory. Let the subsampled point clouds be \hat{S} and \hat{T} .
- 2: Construct the source part-whole graph G_S . Estimate the bounding boxes for each part.
- 3: Run Leopard to discover the set of correspondences \mathcal{K} between \hat{S} and \hat{T} .
- 4: Derive whole body rigid transformation (R_{whole}, t_{whole}) from \hat{S} to \hat{T} using \mathcal{K} . (Section 4.2.6). Apply (R_{whole}, t_{whole}) to S to obtain S' and to \hat{S} to obtain \hat{S}' .
- 5: Sort the parts of S in G_S in the decreasing order of volume. Let the sorted list be $\{p_j^S\}_{j=1}^{n_{parts}^S}$.
- 6: **for** $j = 0, 1, \dots, n_{parts}$ **do**
- 7: Segment out the part of \hat{S}' , that corresponds to $p_j^{S'}$ by extraction just the points that fall within the bounding box of $p_j^{S'}$. We need this step to filter out the potential feature points for $p_j^{S'}$. Let us call this set of feature points $p_j^{\hat{S}'}$.
- 8: Estimate the region of interest in T – the set of points in T that may correspond to $p_j^{S'}$. This set is determined by a bounding box that is the smallest one to enclose all the points in T that correspond to feature points in $p_j^{\hat{S}'}$ and the whole of $p_j^{\hat{S}'}$. Let the set of correspondences for this part be \mathcal{K}_j .
- 9: **while** User not satisfied **do**
- 10: Run RANSAC using the correspondences \mathcal{K}_j to obtain the first-level registration results for $p_j - (R_j, t_j)$.
- 11: **end while**
- 12: **while** User not satisfied **do**
- 13: Run ICP with \mathcal{K}_j and the initial transformation set to (R_j, t_j) from the previous step for second-level registration for part p_j . Record the output transformation – $p_j - (R_j, t_j)$ for part p_j .
- 14: **end while**
- 15: Apply (R_j, t_j) to part $p_j^{S'}$.
- 16: **end for**
- 17: Return $\{(R_i, t_i)\}_{i=1}^{n_{parts}}$.

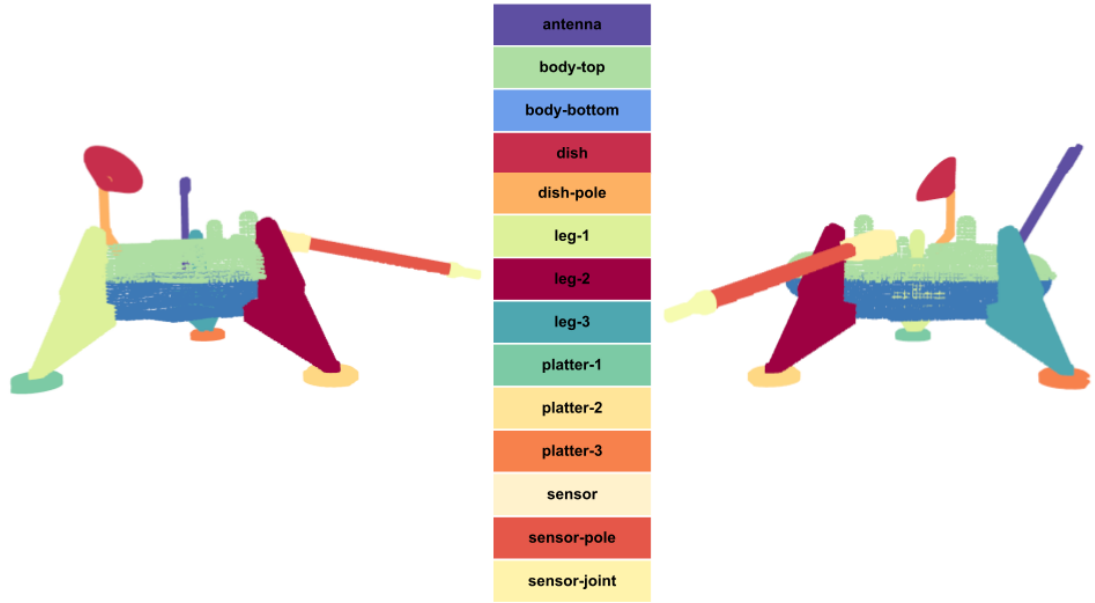


FIGURE 5.1: NASA Viking Lunar Lander with parts labelled. We show two views to reveal the 3D shape of the model.

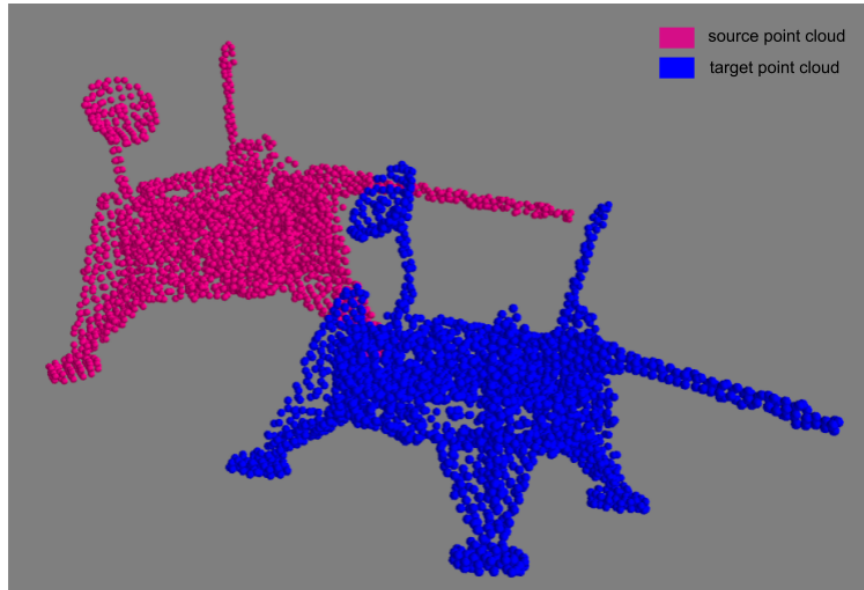


FIGURE 5.2: Source and target point clouds in the example that we use to describe our workflow in this section.

5.4.0.1 Graph representation of source

Our method begins by constructing a bidirectional graph of the source point cloud (which is available as a CAD model). Each node of this graph represents one of the rigid parts. Each pair of adjacent parts is connected with an edge. We illustrate this in figure 5.3.



FIGURE 5.3: Graph Construction of NASA Viking Lunar Lander labelled

5.4.0.2 Correspondence matching using Leopard

In the next step, we run Leopard to obtain the corresponding points in the source and target clouds. Figures 5.6, 5.5, 5.7, and 5.8 show the correspondence matches obtained for some of the lander-parts.

5.4.0.3 Whole body rigid fitting

For rigid fitting, we derive the rigid body transformation for the whole source point cloud. Note that the parts that moved relative to the body resulting in a

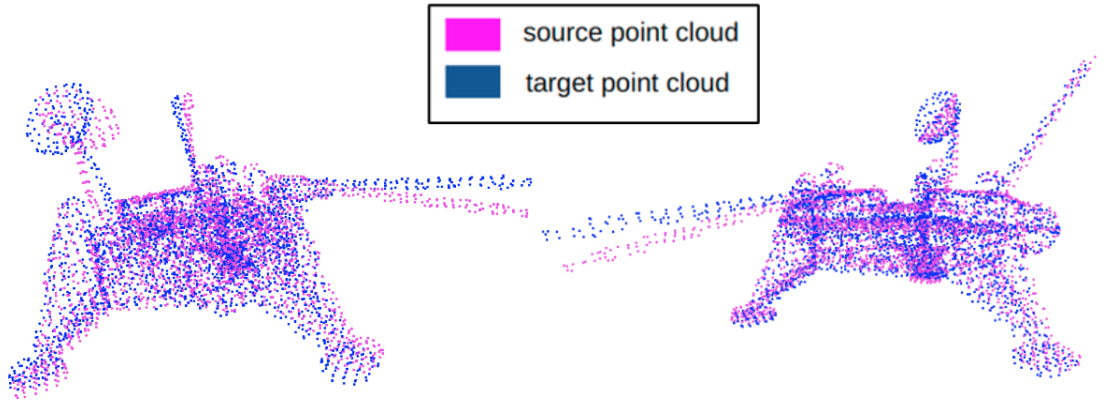


FIGURE 5.4: Point Cloud of NASA Viking Lunar Lander Source and target after Rigid fitting

non-rigid deformation could not be aligned in this step.

5.4.0.4 Part-wise tuning

The next step involves part-wise tuning. We tune the parts in the reverse order of sizes. Each part is tuned in two steps - first using RANSAC () and the correspondences for the feature points in that part. The Leopard pipeline breaks the graph structure of the source point cloud during feature point extraction in the previous step. We recover the feature points for each part using the (axis-aligned) bounding boxes of the part. The output of the RANSAC algorithm is a rotation and translation for the part.

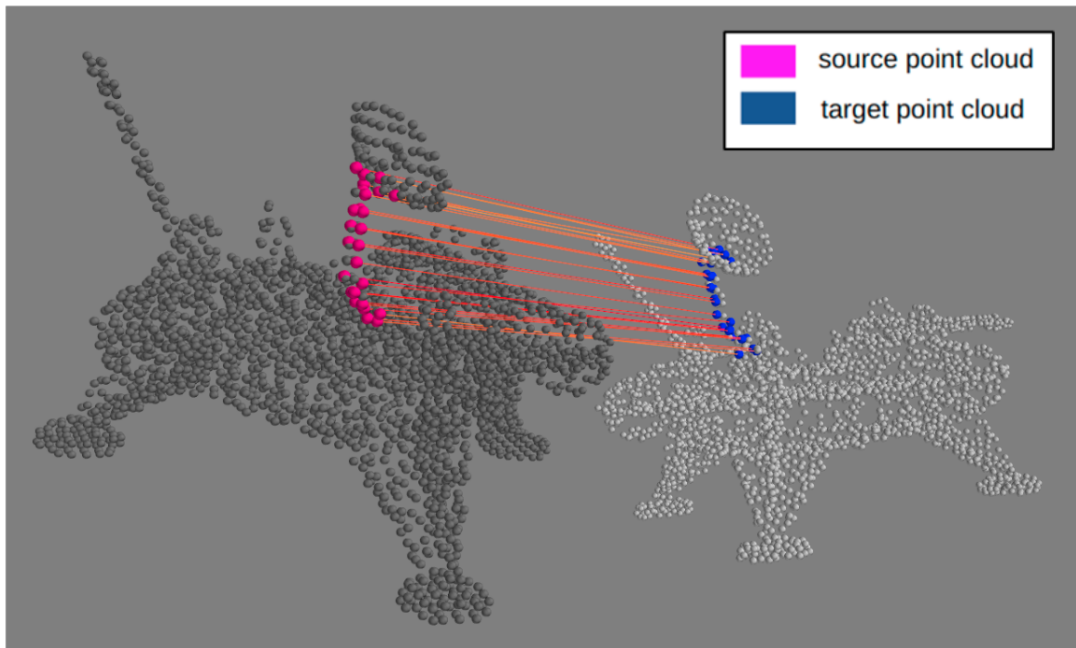


FIGURE 5.5: Correspondences of Dish-pole of NASA Viking Lunar Lander

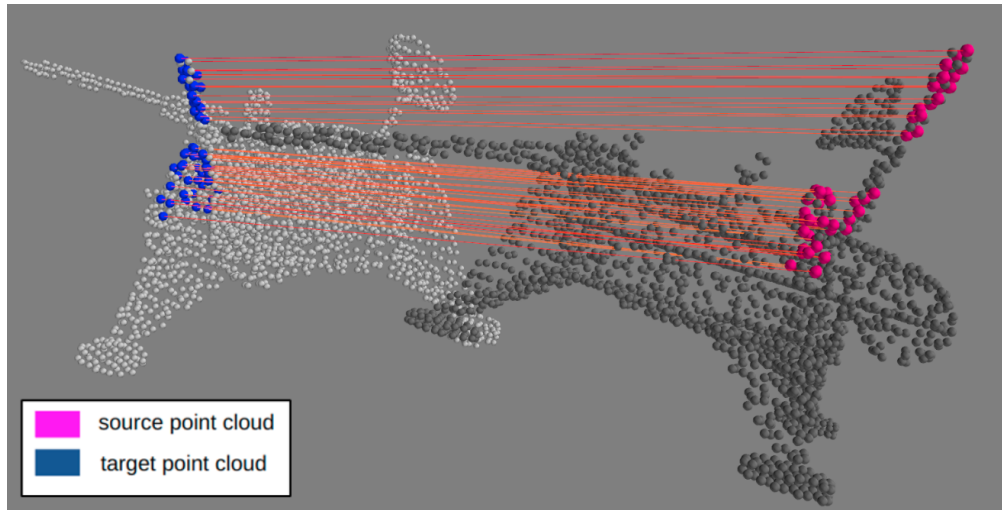


FIGURE 5.6: Correspondences of partial antenna and leg3 of NASA Viking Lunar Lander

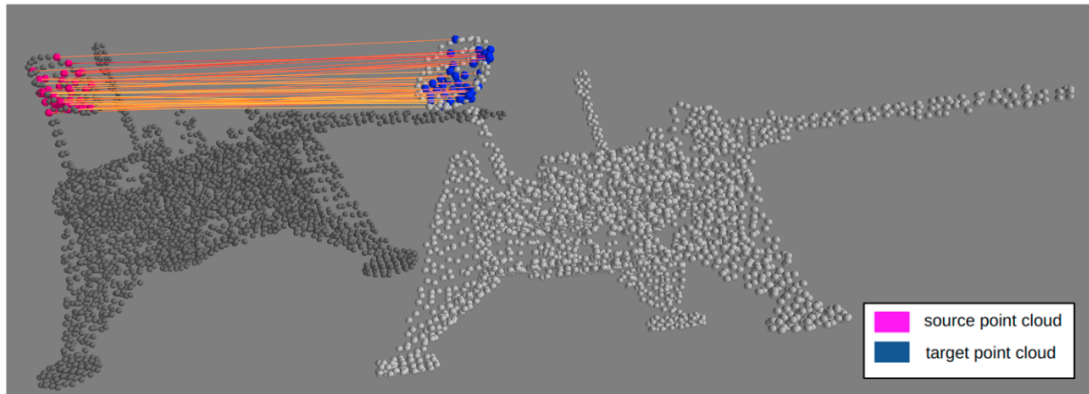


FIGURE 5.7: Correspondences of the dish of NASA Viking Lunar Lander

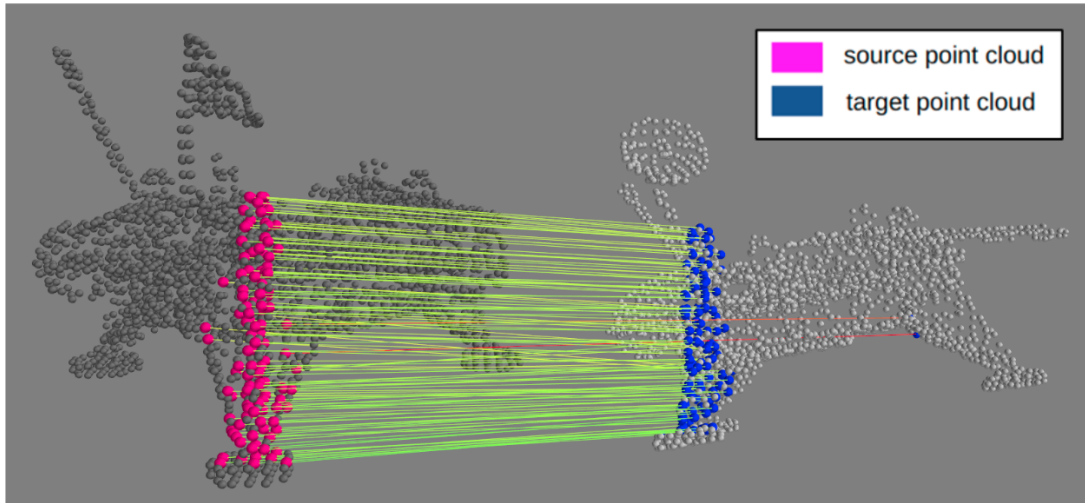


FIGURE 5.8: Correspondences of leg 1 of NASA Viking Lunar Lander

The second step in the tuning process uses ICP to tightly fit the part in its location in the target point cloud. The area of interest in the target point cloud is determined as an axis-aligned bounding box whose extremities cover the axis-aligned bounding box of the source part and all the corresponding points in the target point cloud for the feature points in the source part. Since ICP assumes that the source and target point clouds are spatially close, we initialize the ICP algorithm with the transformation obtained from RANSAC in the previous step. The output of this step is also a rotation and translation for the part in question.

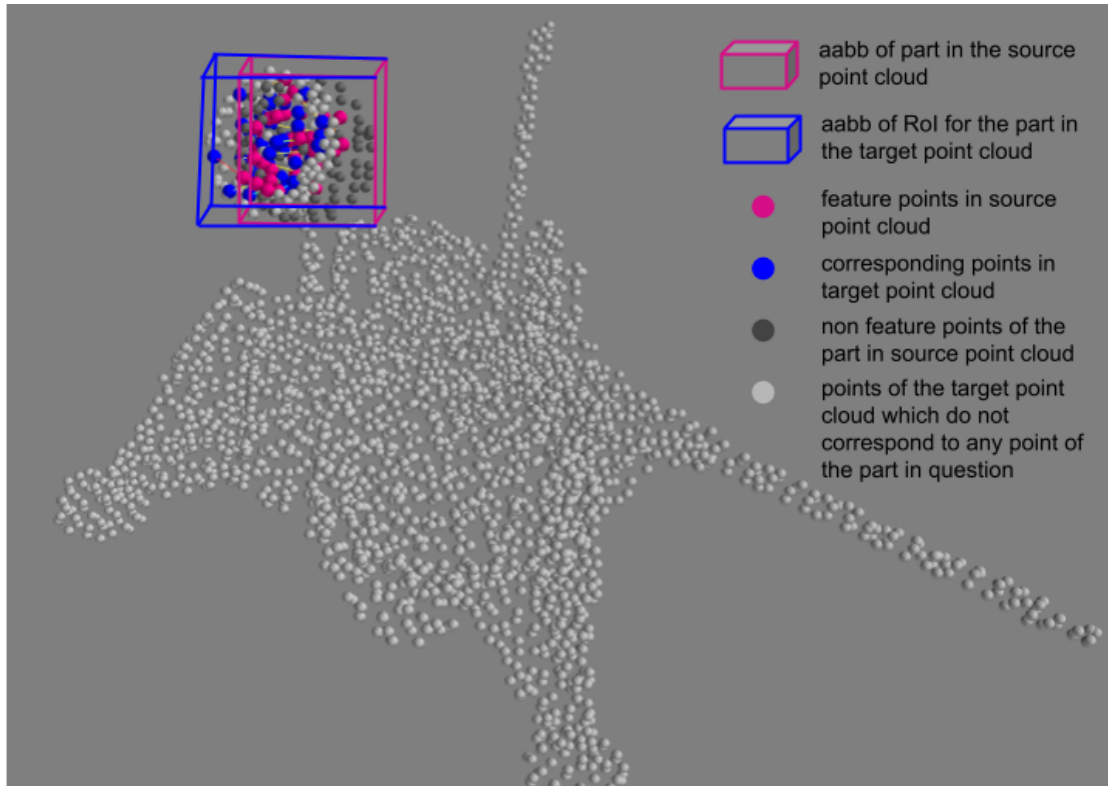


FIGURE 5.9: Diagram showing how we compute the region of interest

We observe that failure to determine the correct region of interest in the target point cloud can adversely affect the performance of the ICP algorithm.

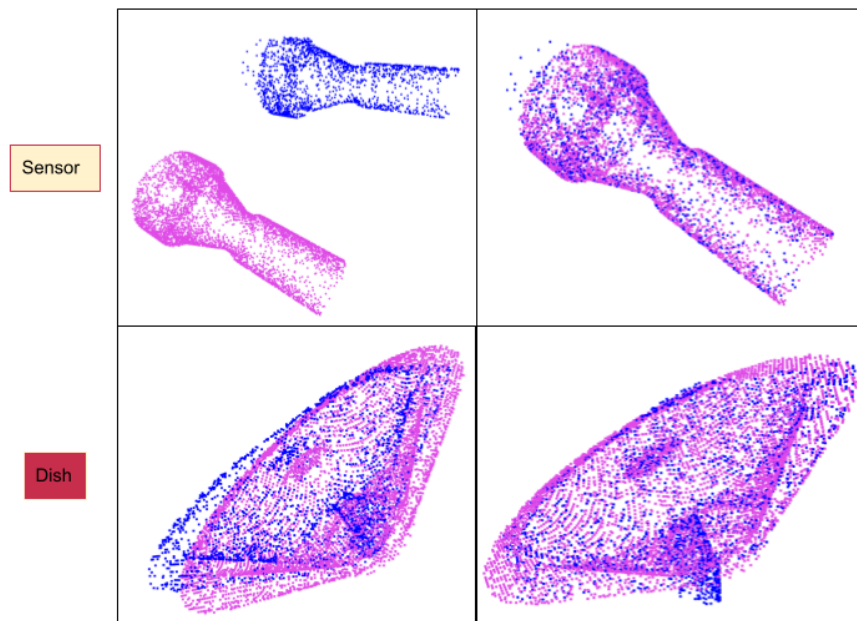


FIGURE 5.10: Results: Left - After RANSAC, Right - After ICP

5.4.1 Final Result

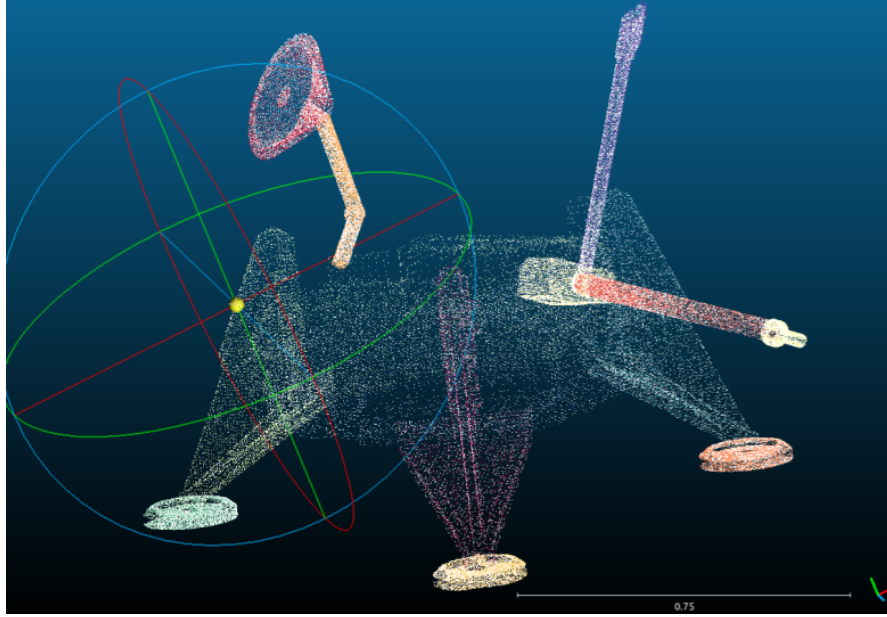


FIGURE 5.11: Final Result after ICP

5.5 Addressing the challenges

1. To prevent the object model from disintegrating upon part-wise transformation we take the following steps:
 - (a) We adjust the parts in decreasing order of sizes.
 - (b) In RANSAC, we add extra correspondences in the form of points that are at the junction of the current part and its larger neighbor that must remain at the same position as they are before the adjustment.
 - (c) If a transformation is causing a joint to be broken, we skip the adjustment
 - (d) If the number of feature points is too low for a given part, we skip the RANSAC step.
2. To make sure that a part is searched for in the right part of the target point cloud, we take the following steps
 - (a) We perform whole body rigid fitting to roughly align the two point clouds.

- (b) Since the output of RANSAC is subject to randomness, we have an interactive interface which keeps repeating the RANSAC step until the user is satisfied with the alignment.
 - (c) We calculate a region of interest in the target point cloud that encompasses the part after rigid registration and all the corresponding points in the target point cloud for the feature points of the part.
3. To take care of outliers:
- (a) KPConv applies a uniform downsampling for preventing the compute load (quadratic in the number of samples) from blowing up. If the density of a point cloud is low, this leads to serious loss in detail and significant degradation in performance. We make sure there are a minimum of 50 points in each part of the input point clouds.
 - (b) We perform fine-tuning with the whole point cloud of the part rather than only the feature points.
 - (c) We perform ICP after RANSAC to correct for the effect of spurious correspondences.

5.6 Conclusion

In this section, we described our proposed algorithm for non-rigid registration for rigid objects with moving parts. We use the example of a NASA Viking Lander model that represents a challenging use case. We explain how the challenges identified in Chapter 4 are addressed in our algorithm. In the following chapter, we present the results of our empirical evaluation.

Chapter 6

Results and Discussion

6.1 Introduction

In Chapters 4 and 5, we presented our proposed method of non-rigid point cloud registration for rigid objects that are composed of movable parts. In this section, we present the results of the empirical evaluation of our approach. We also discuss the key takeaways from the experiments and present some failure modes.

6.2 Experimental Setup

We begin by presenting our experimental setup which includes key open source repositories that we depend upon, data collection and data preparation.

6.2.1 Code base

As explained in Chapter 5, our algorithm builds on top of Lepard (Li & Harada, 2022). We use the official implementation of Lepard from the GitHub repository¹ released by the authors. We used Open3D and Mayavi libraries for visualization. The graph operations were performed using the Python NetworkX library.

¹<https://github.com/rabbityl/lepard>

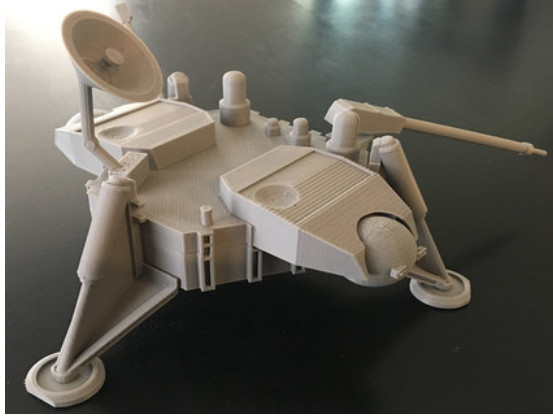


FIGURE 6.1: CAD Model of NASA Viking Lander used as source point cloud in our experiments.

6.2.2 Data collection

We use the trained models open-sourced by the authors of Lepard (Li & Harada, 2022) for demonstrating the performance of our proposed method. There are two models - one trained on the “3DMatch” dataset and one on the “4DMatch” dataset. These datasets are comprised of a wide range of examples of rigid (3DMatch) and non-rigid (4DMatch) registration with varying degrees of noise and percentage of overlap. We discussed these datasets in detail in Section 3.3. As mentioned in Section 4, our test subjects in this thesis are rigid objects with parts that can move about joints. We use 3D printed models of the NASA Viking Lander² and the Cubebot³ as shown in Figures 6.1 and 6.2 as representatives in our experiments. The parts of the NASA Viking Lander and the Cubebot are labelled in Figures 5.1 and 6.3 respectively. The NASA Viking Lander poses the challenge of complex geometry. On the other hand, the Cubebot has all its parts made of cuboids and has a considerably simpler geometry. However, it poses a different set of challenges due to ambiguity between the parts of similar geometry and can test the efficacy of the Lepard (Li & Harada, 2022) pipeline as claimed by the authors. The source point clouds are extracted directly from the CAD models. For scanning the target point cloud, we use Microsoft Hololens 2 (Ungureanu et al., 2020). We set up the workflow shown in Figure 6.4 to ingest Hololens 2 data into the Lepard pipeline.

²Open source model of NASA Viking Lander obtained from <https://nasa3d.arc.nasa.gov/detail/viking-lander>.

³Open source model of Cubebot in a dancing pose obtained from <https://sketchfab.com/3d-models/dancing-cubebot-fe41ed9dce7e41b5a46fed8705a6821e>.

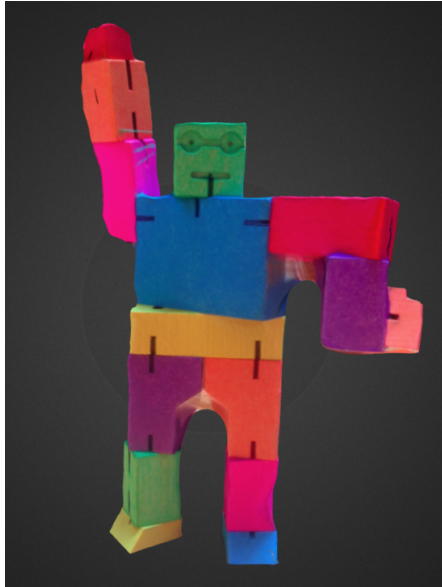


FIGURE 6.2: CAD Model of dancing Cubebot used as source point cloud in our experiments.

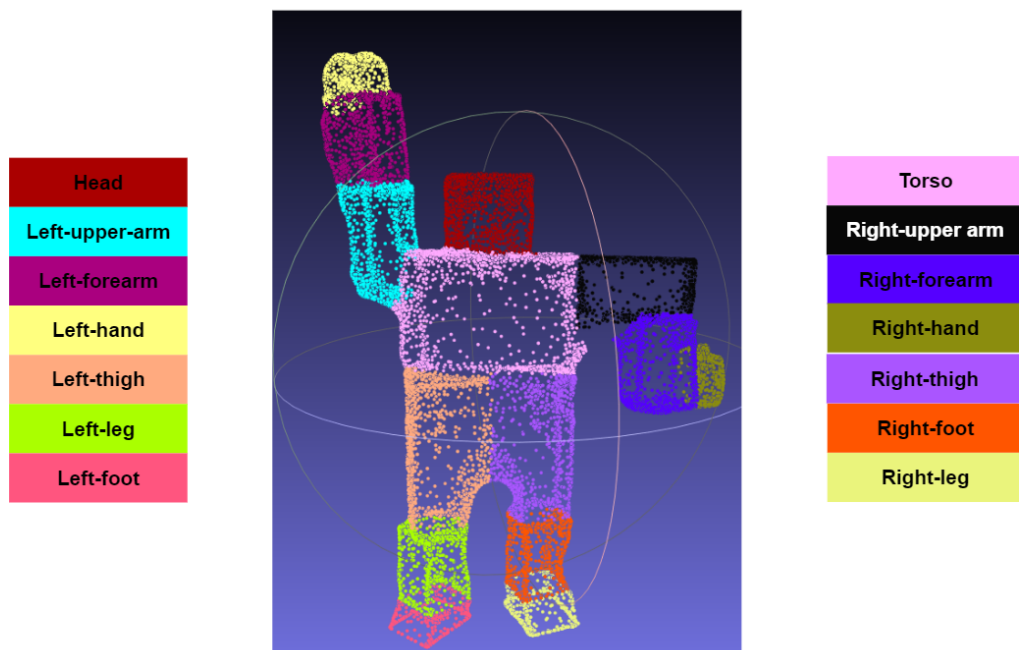


FIGURE 6.3: Cubebot with parts labelled.

6.2.3 Data preparation

The uniform subsampling implemented by KPConv within the Leopard pipeline is sensitive to the scale of the point cloud. Small scans are often lost after the subsampling operation. We scaled the point cloud up by $10\times$ along all three axes to prevent critical data loss. In order to segment out the target object from

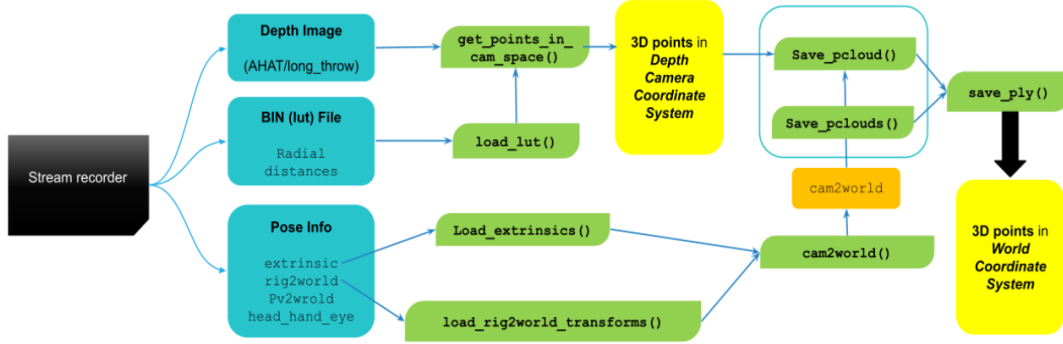


FIGURE 6.4: Pipeline for converting data recorded with Microsoft HoloLens 2 into the input format of Lepard.

background objects and walls in the scanned point cloud from HoloLens 2, we use distance thresholding and DBSCAN clustering (Ester et al., 1996). In the experiments with a low amount of noise, we fuse multiple scans from different angles to obtain a near-complete target point cloud.

6.3 Results

In this section, we present the results of our experiments. We design experiments with progressive levels of difficulty to demonstrate the strengths and weaknesses of our algorithm. Difficulty arises from the number of deformations and degrees of noise in the target point cloud.

6.3.1 Experiment 1: No deformations, low noise

The first experiment is designed to demonstrate the best case scenario of non-rigid registration which is the case of zero deformations and a clean scan of the target point cloud. The source and the target point clouds can be aligned through a whole body rigid transformation.

6.3.1.1 Discussion

Figures 6.5 and 6.8 show the source and target point clouds for NASA Viking Lander and Cubebot respectively. The respective transformed source and target

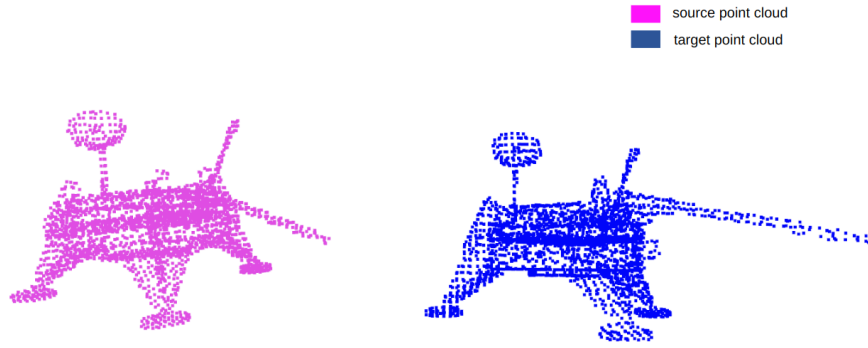


FIGURE 6.5: Source and target point clouds for Experiment 1 in Section 6.3.1 with NASA Viking Lander.

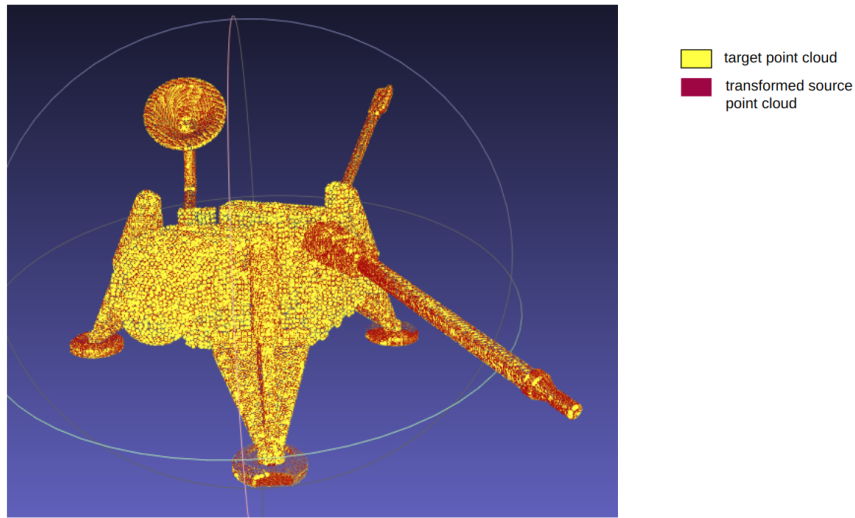


FIGURE 6.6: Transformed source and target point clouds for Experiment 1 in Section 6.3.1 with NASA Viking Lander.

point clouds after registration are in Figures 6.6 and 6.9. Figures 6.7 and 6.10 show the degree of alignment through a map of the nearest neighbor distance between the transformed-source and target point clouds. We observe that our workflow is able to accurately register the source and target point clouds for the degenerate case of no deformations and low noise.

6.3.2 Experiment 2: Non-rigid deformation in one part, low noise

In the second experiment, we introduce a non-rigid deformation in the target point cloud. In the case of NASA Viking Lander, the “dish” along with the “dish-pole”

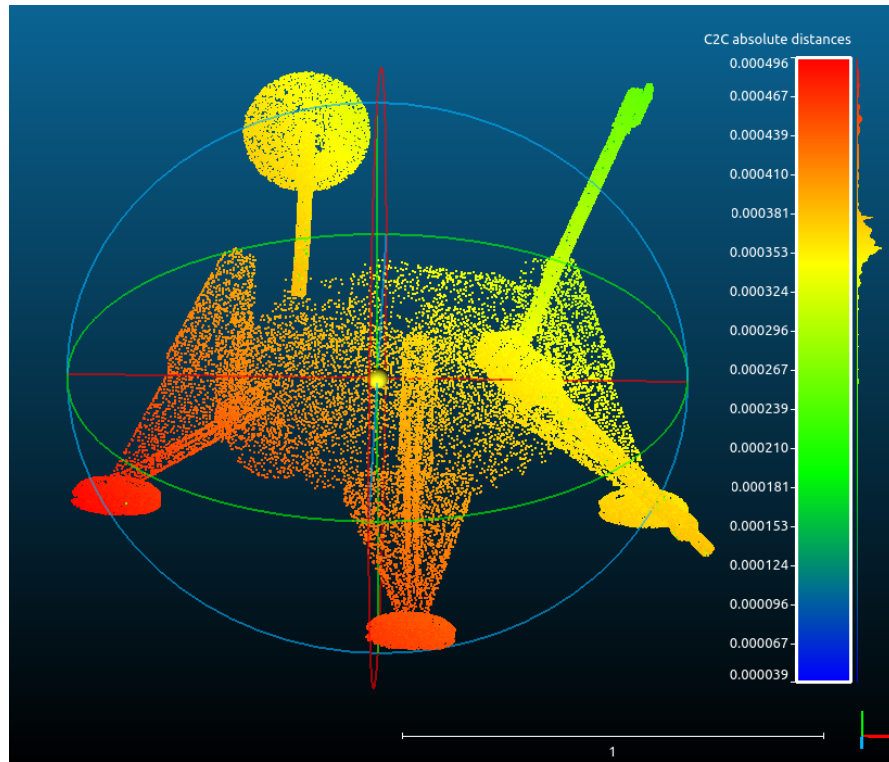


FIGURE 6.7: Visualization alignment of transformed source and target point clouds for Experiment 1 in Section 6.3.1 with NASA Viking Lander. C2C distance is a cloud-to-cloud approximate nearest neighbor distance computed by CloudCompare ([Girardeau-Montaut, 2016](#)).

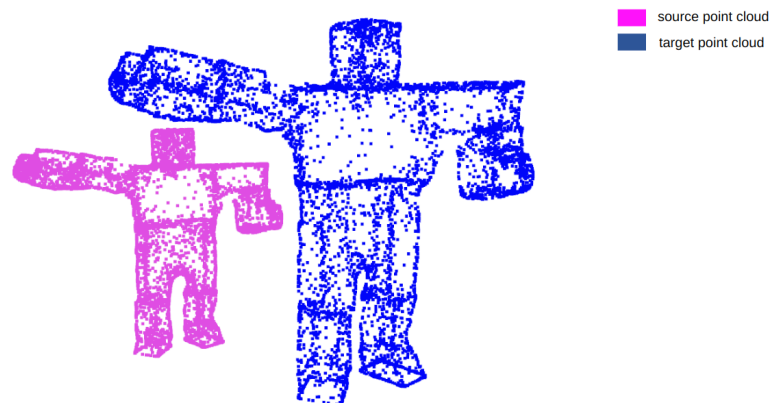


FIGURE 6.8: Source and target point clouds for Experiment 1 in Section 6.3.1 with CubeBot.

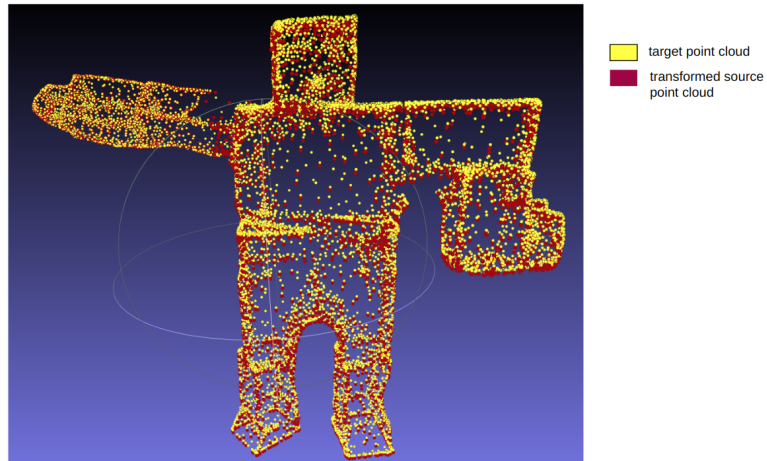


FIGURE 6.9: Transformed source and target point clouds for Experiment 1 in Section 6.3.1 with Cubebot.

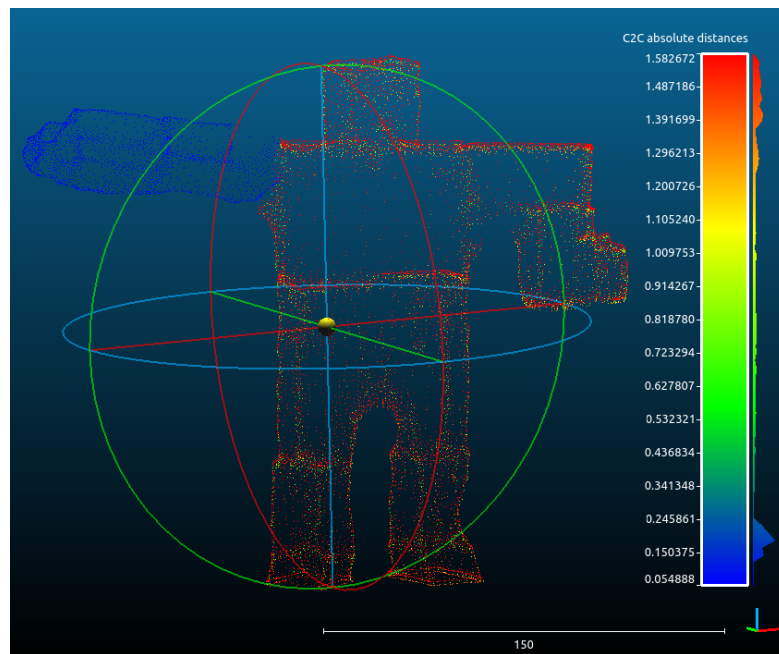


FIGURE 6.10: Visualization alignment of transformed source and target point clouds for Experiment 1 in Section 6.3.1 with Cubebot. C2C distance is a cloud-to-cloud approximate nearest neighbour distance computed by CloudCompare (Girardeau-Montaut, 2016).

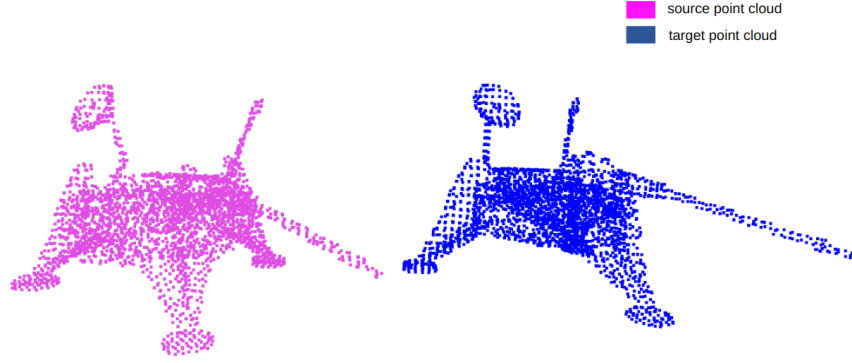


FIGURE 6.11: Source and target point clouds for Experiment 2 in Section 6.3.2 with NASA Viking Lander.

is deformed. In the case of Cubebot, the “left-hand” is deformed. For alignment, we must carry out a whole-body rigid transformation followed by part-wise tuning. In this task, the target scan is clean.

6.3.2.1 Discussion

Figures 6.11 and 6.14 show the source and target point clouds for NASA Viking Lander and Cubebot respectively. The respective transformed source and target point clouds after registration are in Figures 6.12 and 6.15. Figures 6.13 and 6.16 show the degree of alignment through a map of the nearest neighbour distance between the transformed source and target point clouds. We observe that our workflow is able to accurately register the source and target point clouds in the case of the Lander. We can observe a small misalignment around the deformed hand of the Cubebot as can be anticipated in the case of sparse point clouds.

6.3.3 Experiment 3: Non-rigid deformation in multiple parts, low noise

In this experiment, we consider a slightly more difficult and a more generic version of Experiment 2 (Section 6.3.2) where multiple parts of the object undergo non-rigid deformations. In case of the NASA Viking Lander, the “dish”, “dish-pole”, “sensor”, “sensor-base” and “sensor-pole” are deformed. In case of the Cubebot, the “left-hand” and the “left-leg” are deformed.

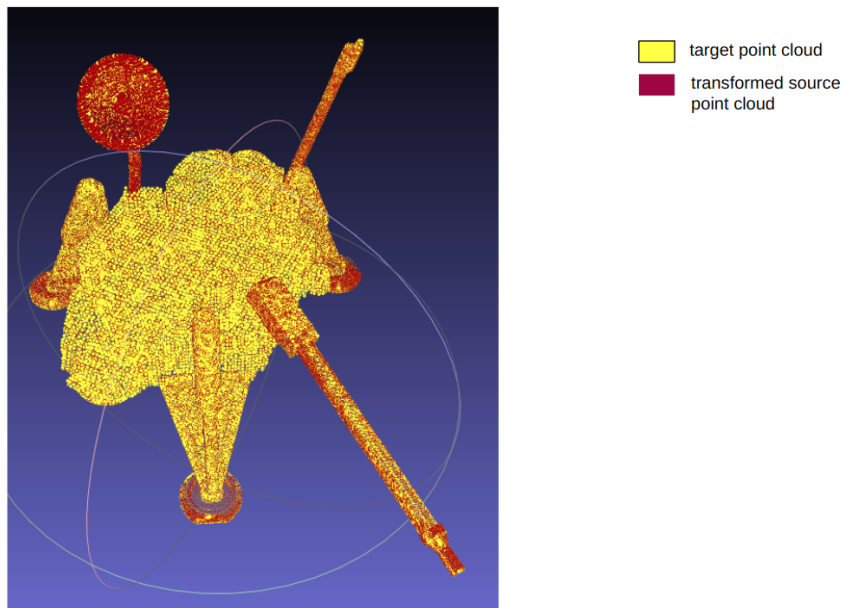


FIGURE 6.12: Transformed source and target point clouds for Experiment 2 in Section 6.3.2 with NASA Viking Lander.

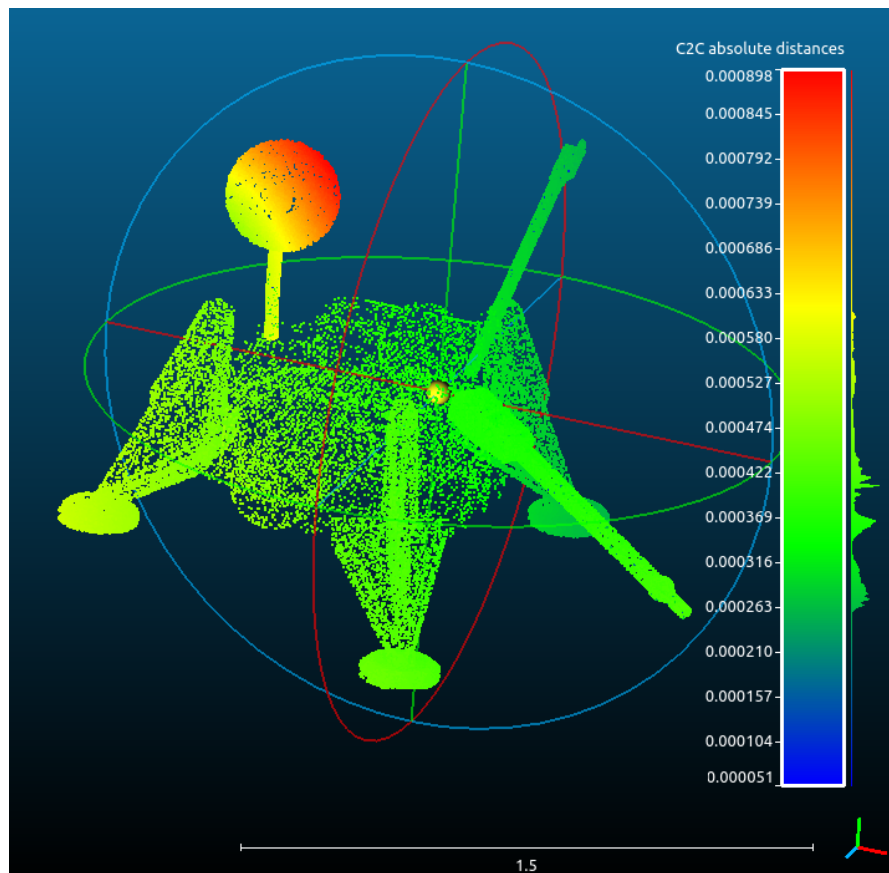


FIGURE 6.13: Visualization alignment of transformed source and target point clouds for Experiment 2 in Section 6.3.2 with NASA Viking Lander. C2C distance is a cloud-to-cloud approximate nearest neighbor distance computed by CloudCompare ([Girardeau-Montaut, 2016](#)).

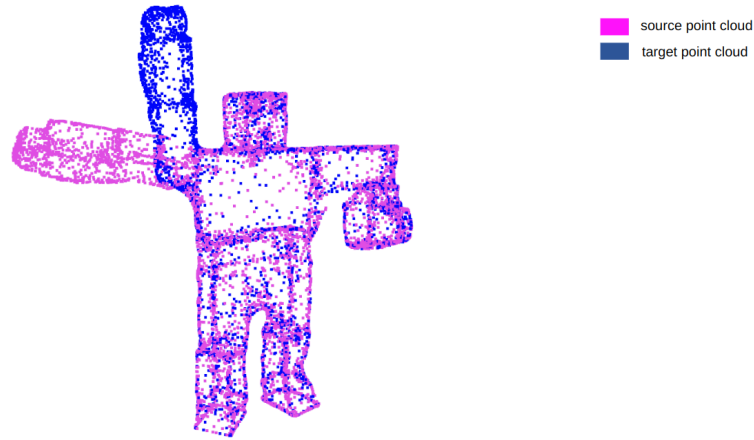


FIGURE 6.14: Source and target point clouds for Experiment 2 in Section 6.3.2 with Cubebot.

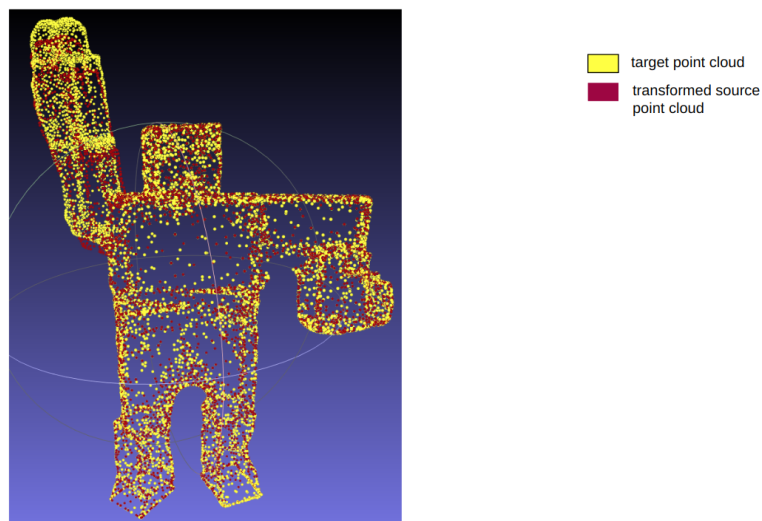


FIGURE 6.15: Transformed source and target point clouds for Experiment 2 in Section 6.3.2 with Cubebot.

6.3.3.1 Discussion

Figures 6.17 and 6.21 show the source and target point clouds for NASA Viking Lander and Cubebot respectively. The respective transformed source and target point clouds after registration are in Figures 6.18 and 6.21. Figures 6.19 and 6.22 show the degree of alignment through a map of the nearest neighbor distance between the transformed-source and target point clouds. We observe that our workflow is able to accurately register the source and target point clouds for the Lander. As in Experiment 2, we can observe a bit of misalignment around in the deformed hand of the Cubebot as can be anticipated in the case of sparse point clouds.

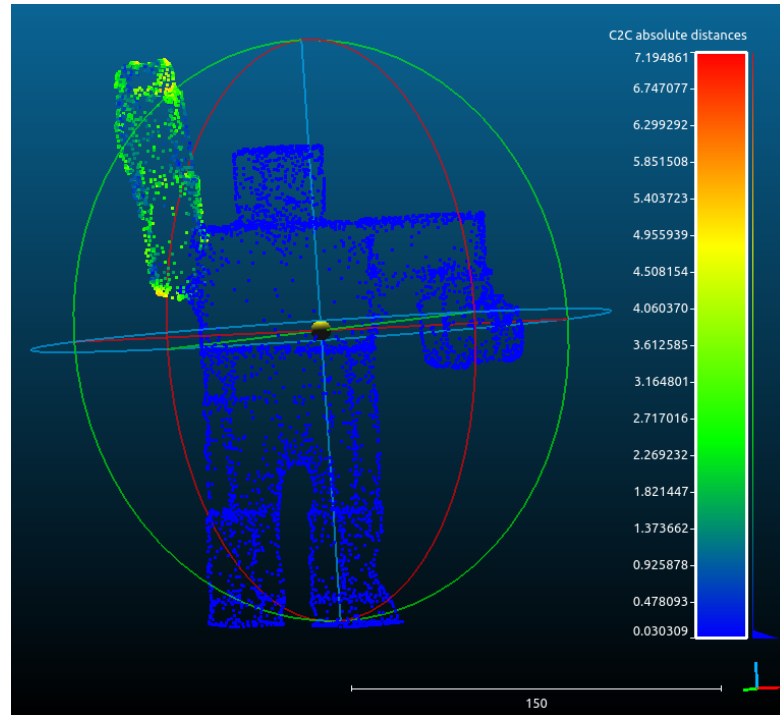


FIGURE 6.16: Visualization alignment of transformed source and target point clouds for Experiment 2 in Section 6.3.2 with Cubebot. C2C distance is a cloud-to-cloud approximate nearest neighbor distance computed by CloudCompare (Girardeau-Montaut, 2016).

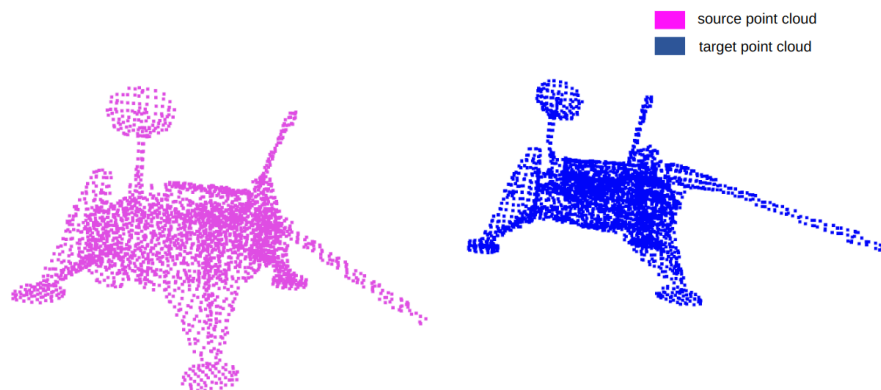


FIGURE 6.17: Source and target point clouds for Experiment 3 in Section 6.3.3 with NASA Viking Lander.

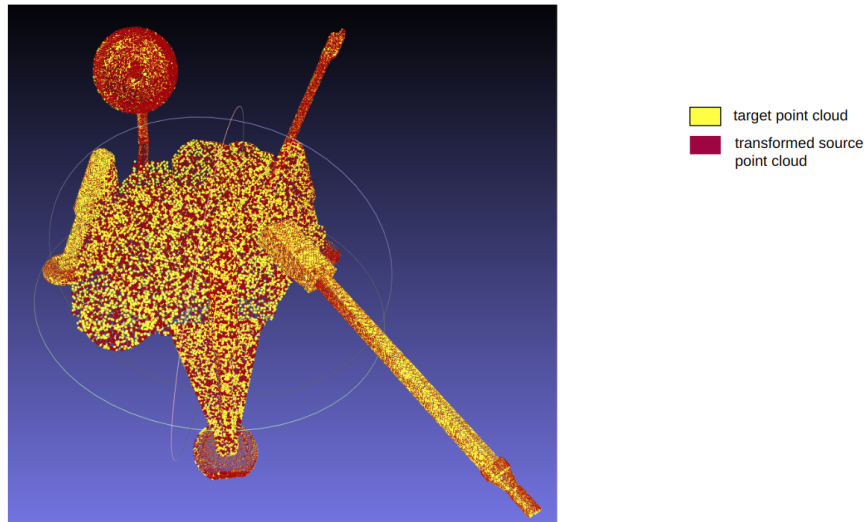


FIGURE 6.18: Transformed source and target point clouds for Experiment 3 in Section 6.3.3 with NASA Viking Lander.

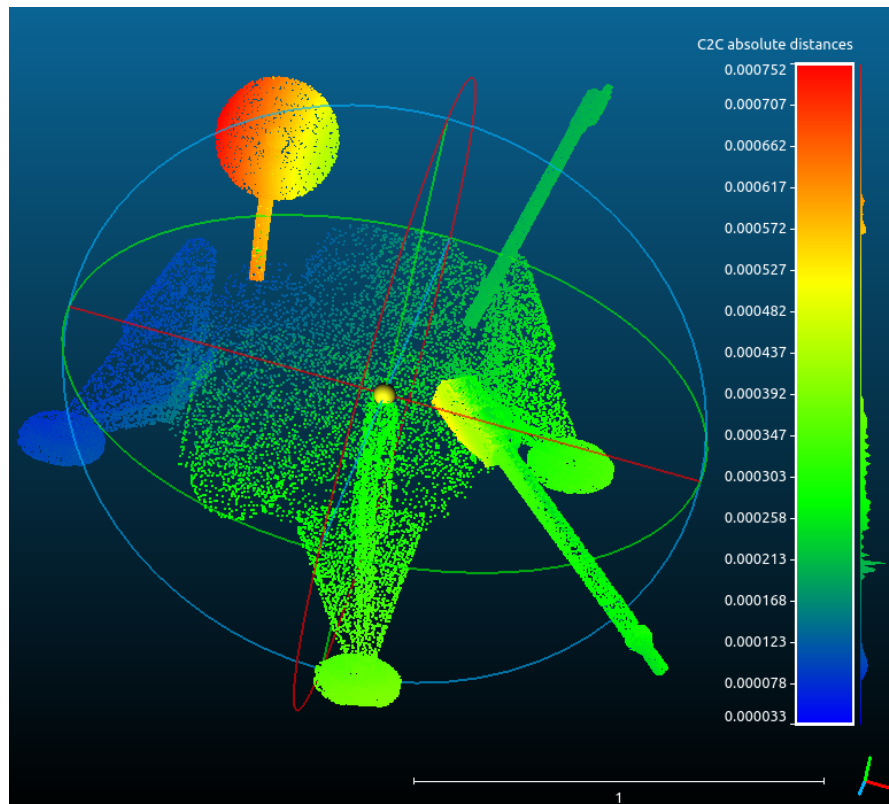


FIGURE 6.19: Visualization alignment of transformed source and target point clouds for Experiment 3 in Section 6.3.3 with NASA Viking Lander. C2C distance is a cloud-to-cloud approximate nearest neighbor distance computed by CloudCompare ([Girardeau-Montaut, 2016](#)).

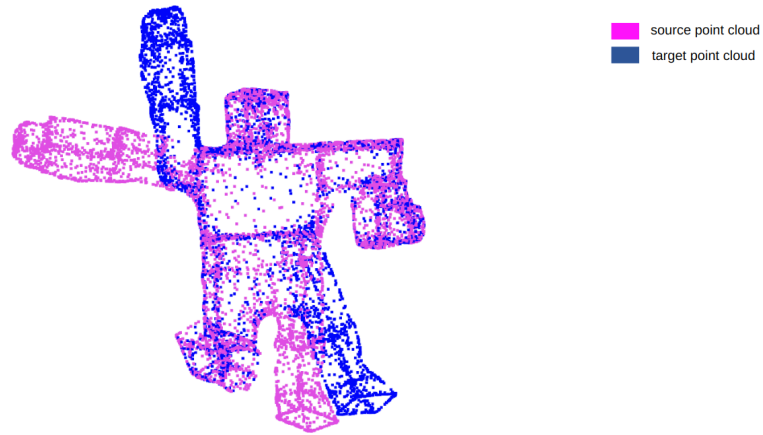


FIGURE 6.20: Source and target point clouds for Experiment 3 in Section 6.3.3 with Cubebot.

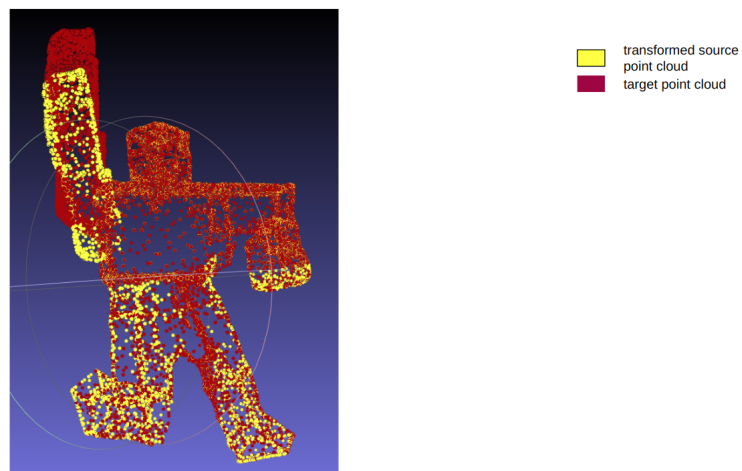


FIGURE 6.21: Transformed source and target point clouds for Experiment 3 in Section 6.3.3 with Cubebot.

6.3.4 Experiment 4: Non-rigid deformation in multiple parts, Noisy target point cloud

This is the most difficult setting where we not only have multiple deformations but also a noisy scan of the target point cloud with holes. This closely mimics real-world use cases in a mixed reality where it is common to have holes and missing parts in a 3D scan. Like Experiment 3, in the case of the NASA Viking Lander, the “dish”, “dish-pole”, “sensor”, “sensor-base” and “sensor-pole” are deformed. In the case of the Cubebot, the “left-hand” and the “left-leg” are deformed.

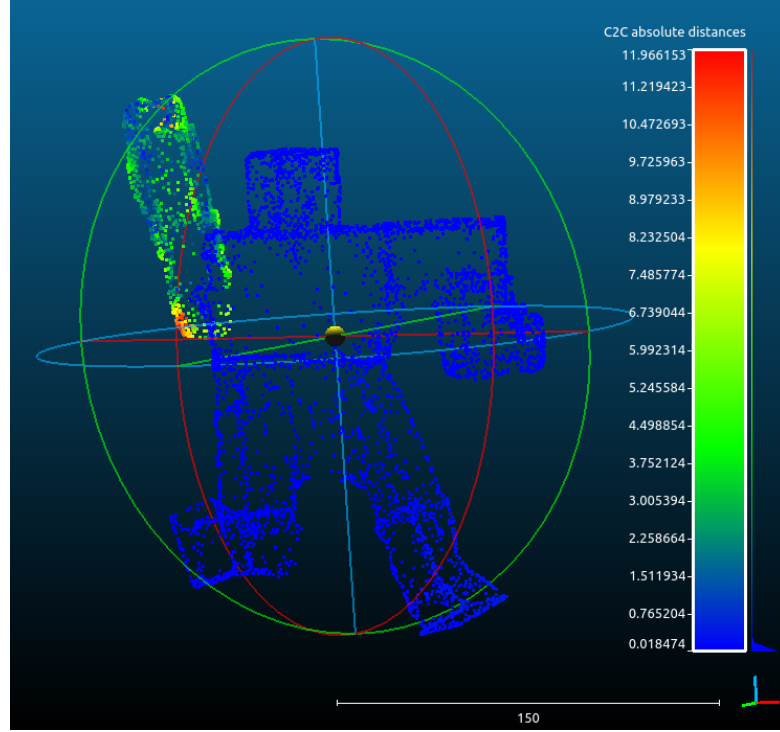


FIGURE 6.22: Visualization alignment of transformed source and target point clouds for Experiment 3 in Section 6.3.3 with Cubebot. C2C distance is a cloud-to-cloud approximate nearest neighbour distance computed by CloudCompare (Girardeau-Montaut, 2016).

6.3.4.1 Discussion

Figures 6.23 and 6.27 shows the source and target point clouds for NASA Viking Lander and Cubebot respectively. The respective transformed source and target point clouds after registration are in Figures 6.24 and 6.27. Figures 6.25 and 6.28 show the degree of alignment through a map of the nearest neighbour distance between the transformed source and target point clouds. We observe that in both cases – Lander and Cubebot – alignment is successful. This demonstrates that our proposed algorithm is robust to noise, holes and missing areas in the target point cloud, and hence is a viable approach for real-world mixed reality applications.

6.4 Hyperparameter values

We present the hyperparameters of our study in Table 6.1.

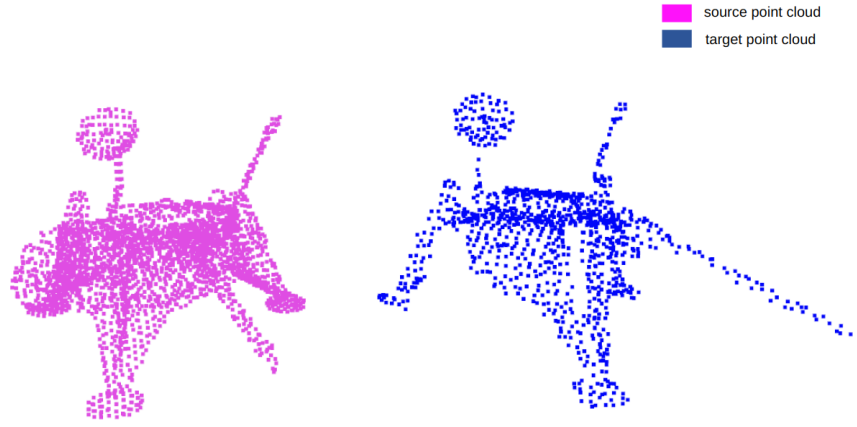


FIGURE 6.23: Source and target point clouds for Experiment 4 in Section 6.3.4 with NASA Viking Lander.

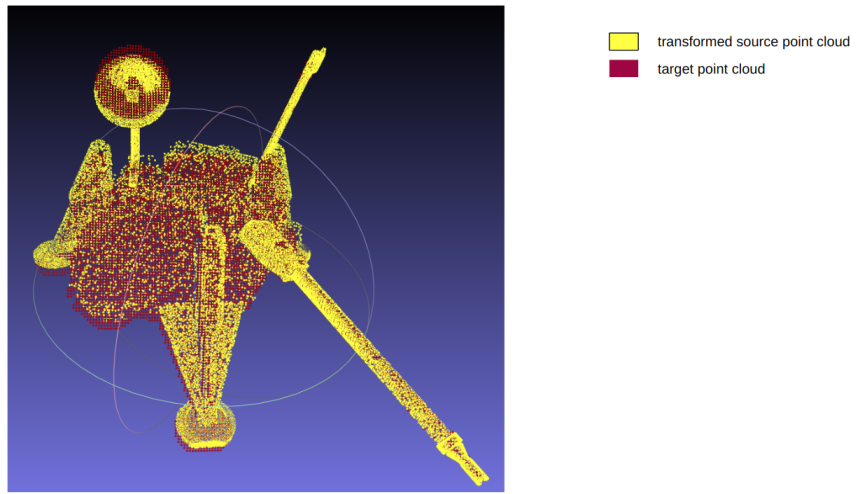


FIGURE 6.24: Transformed source and target point clouds for Experiment 4 in Section 6.3.4 with NASA Viking Lander.

TABLE 6.1: Table of hyperparameters.

Hyperparameter	Values	
	NASA Viking Lander	Cubebot
$f_{\text{retention}}^{\text{subsample}}$	0.5	0.4
$d_{\text{max}}^{\text{corr}}$	20	20
$n_{\text{min}}^{\text{corr}}$	5	5

6.5 Conclusion

In this chapter, we presented the results of empirical evaluation of the approach proposed in Chapter 5. We presented 4 experiments with increasing levels of difficulty on two real world objects that posed two major kinds of difficulty. We

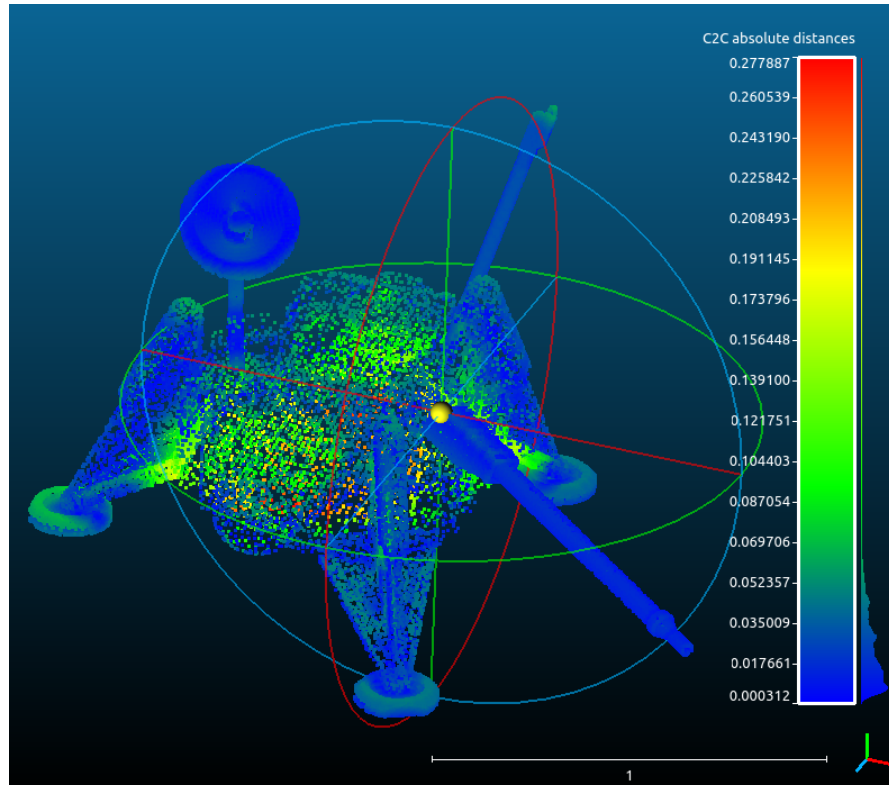


FIGURE 6.25: Visualization alignment of transformed source and target point clouds for Experiment 4 in Section 6.3.4 with NASA Viking Lander. C2C distance is a cloud-to-cloud approximate nearest neighbour distance computed by CloudCompare (Girardeau-Montaut, 2016).

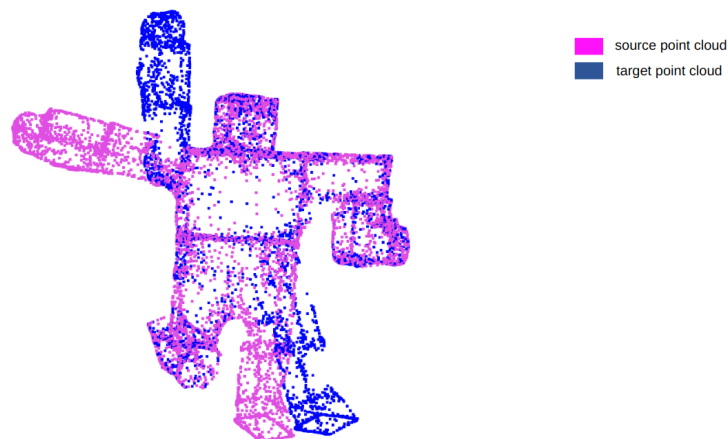


FIGURE 6.26: Source and target point clouds for Experiment 4 in Section 6.3.4 with CubeBot.

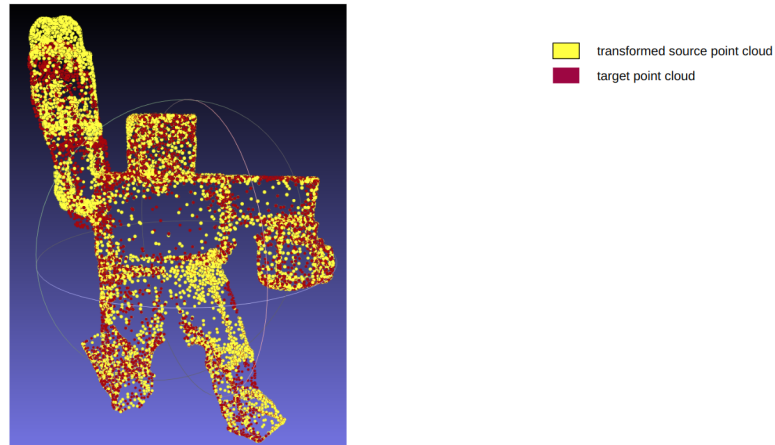


FIGURE 6.27: Transformed source and target point clouds for Experiment 4 in Section 6.3.4 with Cubebot.

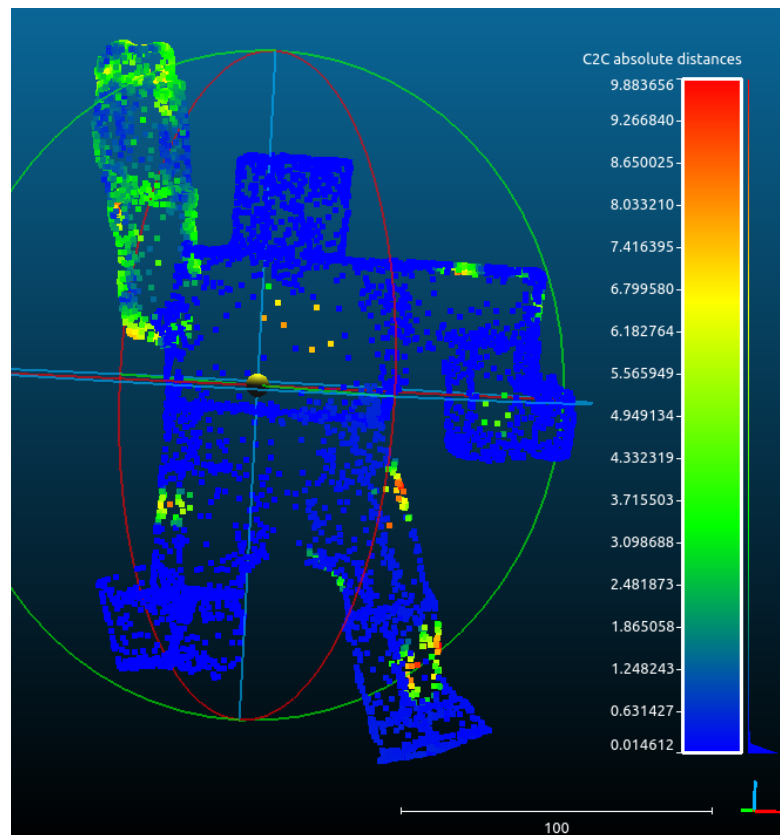


FIGURE 6.28: Visualization alignment of transformed source and target point clouds for Experiment 4 in Section 6.3.4 with Cubebot. C2C distance is a cloud-to-cloud approximate nearest neighbour distance computed by CloudCompare (Girardeau-Montaut, 2016).

demonstrated the robustness of the proposed approach and discussed the failure modes.

Chapter 7

Conclusion

7.1 Introduction

In this section, we conclude the thesis with a recapitulation of the studies presented in the previous chapters. We also discuss the limitations of our approach and motivate future directions of research.

7.2 Summary of achievements

The aim of this thesis was to study point cloud registration in the context of deformable objects and Mixed Reality (MR) applications. We focussed on the task of alignment of CAD models with real world 3D scans as this is the one of the crucial use cases in enterprise MR at the present date. Since real time operation is crucial for a seamless MR experience, we aimed to identify crucial rate-limiting steps and optimize them for our use cases.

Here is a summary of our achievements towards the goals of this thesis:

- We carried out a thorough literature survey of the state-of-the-art point cloud registration algorithms that are capable of dealing with non-rigid deformations between the source and target point clouds.
- We implemented a data capture and rendering pipeline on Microsoft Hololens 2, a leading MR platform.

- We implemented the state-of-the-art non-rigid point cloud matching algorithm - Leopard (Li & Harada, 2022) - and evaluated it on real world scans from Hololens 2.
- We identified the rate limiting step as the non-rigid registration / warping step that came after the inference of feature-point correspondences from the Leopard pipeline.
- We narrowed our scope to objects that are composed of rigid parts that can move relative to one another about hinges and joints. These comprise the most common subjects in non-rigid registration applications in enterprise mixed reality use cases.
- We proposed a fast non-rigid registration workflow that leverages the graph structure of the source CAD model, correspondences predicted by Leopard, RANSAC and ICP and demonstrated high efficacy on our real world test scans even in the presence of noise, holes and missing parts.

7.3 Contribution to knowledge

In this thesis, we made the following findings:

- We discovered that the non-rigid registration step using popular mesh warping methods like N-ICP are very time consuming and prior knowledge about the structure of the source cloud can be leveraged to derive much more efficient non-rigid registration workflow.
- We confirmed the high sensitivity of ICP to noise. A 3-step registration process at the whole body and then at the part level helped in achieving robustness in the workflow.

7.4 Recommendations for future work

The method presented in this thesis strongly leverages the structure of the object. However this might not always be available. An interesting research direction would be to segment the parts of a 3D object that move as a whole by tracking

the movements of the object. This will enable us to use our proposed method for the more generic non-rigid point cloud registration use case.

Bibliography

- Abate A. F., Narducci F., Ricciardi S., 2013, in International Conference on Virtual, Augmented and Mixed Reality Mixed reality environment for mission critical systems servicing and repair. pp 201–210
- Ao S., Hu Q., Yang B., Markham A., Guo Y., 2021, in Proceedings of the IEEE/CVF Conference on Computer Vision and Pattern Recognition Spinnet: Learning a general surface descriptor for 3d point cloud registration. pp 11753–11762
- Aoki Y., Goforth H., Srivatsan R. A., Lucey S., 2019, in Proceedings of the IEEE/CVF conference on computer vision and pattern recognition Pointnetlk: Robust & efficient point cloud registration using pointnet. pp 7163–7172
- Arun K. S., Huang T. S., Blostein S. D., 1987, IEEE Transactions on pattern analysis and machine intelligence, pp 698–700
- Attaiki S., Pai G., Ovsjanikov M., 2021, in 2021 International Conference on 3D Vision (3DV) Dpfm: Deep partial functional maps. pp 175–185
- Atzmon M., Maron H., Lipman Y., 2018, arXiv preprint arXiv:1803.10091
- Bai X., Luo Z., Zhou L., Chen H., Li L., Hu Z., Fu H., Tai C.-L., 2021, in Proceedings of the IEEE/CVF Conference on Computer Vision and Pattern Recognition Pointdsc: Robust point cloud registration using deep spatial consistency. pp 15859–15869
- Bai X., Luo Z., Zhou L., Fu H., Quan L., Tai C.-L., 2020, in Proceedings of the IEEE/CVF conference on computer vision and pattern recognition D3feat: Joint learning of dense detection and description of 3d local features. pp 6359–6367
- Ben-Shabat Y., Lindenbaum M., Fischer A., 2018, IEEE Robotics and Automation Letters, 3, 3145

- Besl P. J., McKay N. D., 1992, in *Sensor fusion IV: control paradigms and data structures* Vol. 1611, Method for registration of 3-d shapes. pp 586–606
- Blomley R., Jutzi B., Weinmann M., 2016, *ISPRS Annals of Photogrammetry, Remote Sensing & Spatial Information Sciences*, 3
- Borsci S., Lawson G., Broome S., 2015, *Computers in Industry*, 67, 17
- Boulch A., Le Saux B., Audebert N., 2017, *3dor@ eurographics*, 3, 1
- Brodu N., Lague D., 2012, *ISPRS journal of photogrammetry and remote sensing*, 68, 121
- Chen L., Day T. W., Tang W., John N. W., 2017, in *2017 IEEE international symposium on mixed and augmented reality (ISMAR)* Recent developments and future challenges in medical mixed reality. pp 123–135
- Choy C., Dong W., Koltun V., 2020, in *Proceedings of the IEEE/CVF conference on computer vision and pattern recognition* Deep global registration. pp 2514–2523
- Choy C., Gwak J., Savarese S., 2019, in *Proceedings of the IEEE/CVF Conference on Computer Vision and Pattern Recognition* 4d spatio-temporal convnets: Minkowski convolutional neural networks. pp 3075–3084
- Choy C., Park J., Koltun V., 2019, in *Proceedings of the IEEE/CVF International Conference on Computer Vision* Fully convolutional geometric features. pp 8958–8966
- Cignoni P., Ranzuglia G., Callieri M., Corsini M., Ganovelli F., Pietroni N., Tarini M., 2011
- Demantké J., Mallet C., David N., Vallet B., 2011, in *Laserscanning Dimensionality based scale selection in 3d lidar point clouds*
- Deng H., Birdal T., Ilic S., 2018a, in *Proceedings of the European Conference on Computer Vision (ECCV)* Ppf-foldnet: Unsupervised learning of rotation invariant 3d local descriptors. pp 602–618
- Deng H., Birdal T., Ilic S., 2018b, in *Proceedings of the IEEE conference on computer vision and pattern recognition* Ppfnet: Global context aware local features for robust 3d point matching. pp 195–205

- Durrant-Whyte H., Bailey T., 2006, IEEE robotics & automation magazine, 13, 99
- El Banani M., Gao L., Johnson J., 2021, in Proceedings of the IEEE/CVF Conference on Computer Vision and Pattern Recognition Unsupervisedr&r: Unsupervised point cloud registration via differentiable rendering. pp 7129–7139
- Ester M., Kriegel H.-P., Sander J., Xu X., et al., 1996, in kdd Vol. 96, A density-based algorithm for discovering clusters in large spatial databases with noise.. pp 226–231
- Filin S., Pfeifer N., 2005, Photogrammetric Engineering & Remote Sensing, 71, 743
- Girardeau-Montaut D., 2016, France: EDF R&D Telecom ParisTech, 11
- Glasmachers T., 2017, in Asian conference on machine learning Limits of end-to-end learning. pp 17–32
- Goodfellow I., Bengio Y., Courville A., 2016, Deep learning. MIT press
- Graham B., Engelcke M., Van Der Maaten L., 2018, in Proceedings of the IEEE conference on computer vision and pattern recognition 3d semantic segmentation with submanifold sparse convolutional networks. pp 9224–9232
- Groh F., Wieschollek P., Lensch H., 2018, in Asian Conference on Computer Vision Flex-convolution. pp 105–122
- Groueix T., Fisher M., Kim V. G., Russell B. C., Aubry M., 2018, in Proceedings of the European Conference on Computer Vision (ECCV) 3d-coded: 3d correspondences by deep deformation. pp 230–246
- Guo B., Huang X., Zhang F., Sohn G., 2015, ISPRS Journal of Photogrammetry and Remote Sensing, 100, 71
- Hackel T., Wegner J. D., Schindler K., 2016, ISPRS annals of the photogrammetry, remote sensing and spatial information sciences, 3, 177
- Holz D., Ichim A. E., Tombari F., Rusu R. B., Behnke S., 2015, IEEE Robotics & Automation Magazine, 22, 110

- Hua B.-S., Tran M.-K., Yeung S.-K., 2018, in Proceedings of the IEEE conference on computer vision and pattern recognition Pointwise convolutional neural networks. pp 984–993
- Huang J., Birdal T., Gojcic Z., Guibas L. J., Hu S.-M., 2022, IEEE Transactions on Pattern Analysis and Machine Intelligence
- Huang Q.-X., Adams B., Wicke M., Guibas L. J., 2008, in Computer Graphics Forum Vol. 27, Non-rigid registration under isometric deformations. pp 1449–1457
- Huang S., Gojcic Z., Usvyatsov M., Wieser A., Schindler K., 2021, in Proceedings of the IEEE/CVF Conference on computer vision and pattern recognition Predator: Registration of 3d point clouds with low overlap. pp 4267–4276
- Huang W., Alem L., Tecchia F., Duh H. B.-L., 2018, Journal on Multimodal User Interfaces, 12, 77
- Hunter J. D., 2007, Computing in science & engineering, 9, 90
- Jain S., Werth D., 2019, in International Conference on Human-Computer Interaction Current state of mixed reality technology for digital retail: a literature review. pp 22–37
- Jerald J., Giokaris P., Woodall D., Hartbolt A., Chandak A., Kuntz S., 2014, in 2014 IEEE Virtual Reality (VR) Developing virtual reality applications with unity. pp 1–3
- Jutzi B., Gross H., 2009, The International Archives of the Photogrammetry, Remote Sensing and Spatial Information Sciences, 38, 4
- Kent L., Snider C., Gopsill J., Hicks B., 2021, Design Studies, 77, 101046
- Kersten-Oertel M., Jannin P., Collins D. L., 2013, Computerized Medical Imaging and Graphics, 37, 98
- Kirkley S. E., Kirkley J. R., 2005, TechTrends, 49, 42
- Ladwig P., Geiger C., 2018, in International Conference on Remote Engineering and Virtual Instrumentation A literature review on collaboration in mixed reality. pp 591–600

- Lalonde J.-F., Unnikrishnan R., Vandapel N., Hebert M., 2005, in Fifth International Conference on 3-D Digital Imaging and Modeling (3DIM'05) Scale selection for classification of point-sampled 3d surfaces. pp 285–292
- Lawin F. J., Danelljan M., Tosteberg P., Bhat G., Khan F. S., Felsberg M., 2017, in International Conference on Computer Analysis of Images and Patterns Deep projective 3d semantic segmentation. pp 95–107
- Lee I., Schenk T., 2002, International Archives of Photogrammetry Remote Sensing and Spatial Information Sciences, 34, 193
- Li H., Sumner R. W., Pauly M., 2008, in Computer graphics forum Vol. 27, Global correspondence optimization for non-rigid registration of depth scans. pp 1421–1430
- Li J., Chen B. M., Lee G. H., 2018, in Proceedings of the IEEE conference on computer vision and pattern recognition So-net: Self-organizing network for point cloud analysis. pp 9397–9406
- Li X., Kaesemodel Pontes J., Lucey S., 2021, Advances in Neural Information Processing Systems, 34, 7838
- Li Y., Harada T., 2022, in Proceedings of the IEEE/CVF Conference on Computer Vision and Pattern Recognition Leopard: Learning partial point cloud matching in rigid and deformable scenes. pp 5554–5564
- Li Y., Takehara H., Taketomi T., Zheng B., Nießner M., 2021, in Proceedings of the IEEE/CVF International Conference on Computer Vision 4dcomplete: Non-rigid motion estimation beyond the observable surface. pp 12706–12716
- Linsen L., Prautzsch H., 2001, in Eurographics (Short Presentations) Local versus global triangulations.
- Liu X., Han Z., Liu Y.-S., Zwicker M., 2019, in Proceedings of the AAAI Conference on Artificial Intelligence Vol. 33, Point2sequence: Learning the shape representation of 3d point clouds with an attention-based sequence to sequence network. pp 8778–8785
- Liu X., Qi C. R., Guibas L. J., 2019, in Proceedings of the IEEE/CVF conference on computer vision and pattern recognition Flownet3d: Learning scene flow in 3d point clouds. pp 529–537

- Mallet C., Bretar F., Roux M., Soergel U., Heipke C., 2011, *ISPRS journal of photogrammetry and remote sensing*, 66, S71
- Maturana D., Scherer S., 2015, in 2015 IEEE/RSJ international conference on intelligent robots and systems (IROS) Voxnet: A 3d convolutional neural network for real-time object recognition. pp 922–928
- Mitra N. J., Nguyen A., 2003, in Proceedings of the nineteenth annual symposium on Computational geometry Estimating surface normals in noisy point cloud data. pp 322–328
- Mueller D., Ferreira J. M., 2003, in Proceedings of the Technology Enhanced Learning International Conference (TEL 03) Marvel: A mixed-reality learning environment for vocational training in mechatronics
- Munoz D., Bagnell J. A., Vandapel N., Hebert M., 2009, in 2009 IEEE Conference on Computer Vision and Pattern Recognition Contextual classification with functional max-margin markov networks. pp 975–982
- Newcombe R. A., Fox D., Seitz S. M., 2015, in Proceedings of the IEEE conference on computer vision and pattern recognition Dynamicfusion: Reconstruction and tracking of non-rigid scenes in real-time. pp 343–352
- Niemeyer J., Rottensteiner F., Soergel U., 2014, *ISPRS journal of photogrammetry and remote sensing*, 87, 152
- Osada R., Funkhouser T., Chazelle B., Dobkin D., 2002, *ACM Transactions on Graphics (TOG)*, 21, 807
- Ovsjanikov M., Ben-Chen M., Solomon J., Butscher A., Guibas L., 2012, *ACM Transactions on Graphics (ToG)*, 31, 1
- Pais G. D., Ramalingam S., Govindu V. M., Nascimento J. C., Chellappa R., Miraldo P., 2020, in Proceedings of the IEEE/CVF conference on computer vision and pattern recognition 3dregnet: A deep neural network for 3d point registration. pp 7193–7203
- Pauly M., Keiser R., Gross M., 2003, in *Computer graphics forum Vol. 22*, Multi-scale feature extraction on point-sampled surfaces. pp 281–289
- Puy G., Boulch A., Marlet R., 2020, in European conference on computer vision Flot: Scene flow on point clouds guided by optimal transport. pp 527–544

- Qi C. R., Su H., Mo K., Guibas L. J., 2017, in Proceedings of the IEEE conference on computer vision and pattern recognition Pointnet: Deep learning on point sets for 3d classification and segmentation. pp 652–660
- Qi C. R., Yi L., Su H., Guibas L. J., 2017, Advances in neural information processing systems, 30
- Ramachandran P., Varoquaux G., 2011, Computing in Science & Engineering, 13, 40
- Rawat W., Wang Z., 2017, Neural computation, 29, 2352
- Riegler G., Osman Ulusoy A., Geiger A., 2017, in Proceedings of the IEEE conference on computer vision and pattern recognition Octnet: Learning deep 3d representations at high resolutions. pp 3577–3586
- Rodolà E., Cosmo L., Bronstein M., Torsello A., Cremers D., , 2017, Partial functional correspondence In Computer Graphics Forum
- Rokhsaritalemi S., Sadeghi-Niaraki A., Choi S.-M., 2020, Applied Sciences, 10, 636
- Roynard X., Deschaud J.-E., Goulette F., 2018, arXiv preprint arXiv:1804.03583
- Rusu R. B., Blodow N., Beetz M., 2009, in 2009 IEEE international conference on robotics and automation Fast point feature histograms (fpfh) for 3d registration. pp 3212–3217
- Schmidt A., Niemeyer J., Rottensteiner F., Soergel U., 2014, IEEE Geoscience and Remote Sensing Letters, 11, 1614
- Schmidt T., Newcombe R., Fox D., 2016, IEEE Robotics and Automation Letters, 2, 420
- Schnabel R., Wahl R., Klein R., 2007, in Computer graphics forum Vol. 26, Efficient ransac for point-cloud shape detection. pp 214–226
- Singh R. D., Mittal A., Bhatia R. K., 2019, Multimedia Tools and Applications, 78, 15951
- Speicher M., Hall B. D., Nebeling M., 2019, in Proceedings of the 2019 CHI conference on human factors in computing systems What is mixed reality?. pp 1–15

- Su H., Maji S., Kalogerakis E., Learned-Miller E., 2015, in Proceedings of the IEEE international conference on computer vision Multi-view convolutional neural networks for 3d shape recognition. pp 945–953
- Su J., Lu Y., Pan S., Wen B., Liu Y., 2021, arXiv preprint arXiv:2104.09864
- Thomas H., Qi C. R., Deschaud J.-E., Marcotegui B., Goulette F., Guibas L. J., 2019, in Proceedings of the IEEE/CVF international conference on computer vision Kpconv: Flexible and deformable convolution for point clouds. pp 6411–6420
- Ungureanu D., Bogo F., Galliani S., Sama P., Duan X., Meekhof C., Stühmer J., Cashman T. J., Tekin B., Schönberger J. L., et al., 2020, arXiv preprint arXiv:2008.11239
- Vaswani A., Shazeer N., Parmar N., Uszkoreit J., Jones L., Gomez A. N., Kaiser L., Polosukhin I., 2017, Advances in neural information processing systems, 30
- Verma N., Boyer E., Verbeek J., 2018, in Proceedings of the IEEE conference on computer vision and pattern recognition Feastnet: Feature-steered graph convolutions for 3d shape analysis. pp 2598–2606
- Wang X., Dunston P. S., Skiniewski M., 2004, in Proceedings of the 21st International Symposium on Automation and Robotics in Construction (ISARC 2004) Mixed reality technology applications in construction equipment operator training. pp 21–25
- Wang Y., Sun Y., Liu Z., Sarma S. E., Bronstein M. M., Solomon J. M., 2019, Acm Transactions On Graphics (tog), 38, 1
- Weinmann M., Jutzi B., Hinz S., Mallet C., 2015, ISPRS Journal of Photogrammetry and Remote Sensing, 105, 286
- Weinmann M., Jutzi B., Mallet C., Weinmann M., 2017, ISPRS Annals of Photogrammetry, Remote Sensing & Spatial Information Sciences, 4
- Weinmann M., Schmidt A., Mallet C., Hinz S., Rottensteiner F., Jutzi B., 2015, ISPRS Annals of the Photogrammetry, Remote Sensing and Spatial Information Sciences II-3 (2015), Nr. W4, 2, 271

- West K. F., Webb B. N., Lersch J. R., Pothier S., Triscari J. M., Iverson A. E., 2004, in Automatic Target Recognition XIV Vol. 5426, Context-driven automated target detection in 3d data. pp 133–143
- Xu H., Liu S., Wang G., Liu G., Zeng B., 2021, in Proceedings of the IEEE/CVF International Conference on Computer Vision Omnet: Learning overlapping mask for partial-to-partial point cloud registration. pp 3132–3141
- Xu Y., Fan T., Xu M., Zeng L., Qiao Y., 2018, in Proceedings of the European Conference on Computer Vision (ECCV) Spidercnn: Deep learning on point sets with parameterized convolutional filters. pp 87–102
- Yu H., Li F., Saleh M., Busam B., Ilic S., 2021, Advances in Neural Information Processing Systems, 34, 23872
- Zeng A., Song S., Nießner M., Fisher M., Xiao J., Funkhouser T., 2017, in Proceedings of the IEEE conference on computer vision and pattern recognition 3dmatch: Learning local geometric descriptors from rgb-d reconstructions. pp 1802–1811
- Zhang Z., 1994, International journal of computer vision, 13, 119
- Zhou Q.-Y., Park J., Koltun V., 2016, in European conference on computer vision Fast global registration. pp 766–782
- Zhou Q.-Y., Park J., Koltun V., 2018, arXiv preprint arXiv:1801.09847
- Zollhöfer M., Nießner M., Izadi S., Rehmann C., Zach C., Fisher M., Wu C., Fitzgibbon A., Loop C., Theobalt C., et al., 2014, ACM Transactions on Graphics (ToG), 33, 1

Appendix A

Research Proposal



Liverpool John Moores University

Non-Rigid 3D Point Cloud Registration with Applications in Mixed Reality

Research Proposal

by

Manorama Jha

for

Master of Science in Machine Learning

A.1 Summary of the Proposed Research

In this project we aim to study the problem of non-rigid partial point cloud registration for Mixed Reality applications. Mixed Reality (MR) is transforming the industry by providing unique opportunities in engineering design, remote operations and collaboration. We specifically intend to implement a state-of-the-art point cloud registration algorithm - Lepard (Li & Harada, 2022) - on Microsoft HoloLens 2 Mixed Reality Platform (Ungureanu et al., 2020) and investigate potential causes of drift and latency bottlenecks in real-world MR use cases. The anticipated outcomes of this research project are a detailed account of failure modes of Lepard and related algorithms and a robust and fast inference pipeline that is robust to outliers and noise in real-life 3D scans and capable of supporting real-time Mixed Reality applications.

A.2 Research Question

In this thesis we will address the following research question:

“Can we make state-of-the-art non-rigid point cloud registration algorithms robust and low-latency for Mixed Reality use cases in real-world environments?”

A.3 Aim and Objectives

In this thesis, we aim to study the problem of 3D Point Cloud Registration for non-rigid objects. Apart from wide-spread relevance in computer vision, robotics and medical science this problem statement is central in many Mixed Reality applications. Although significant advancements have been made in 3D representation learning and computer vision in recent years, several engineering challenges stand in the way of deploying these algorithms at scale. The objectives of this thesis are as follows:

1. Prepare a thorough literature review of prominent approaches to 3D Point Cloud Registration with emphasis on non-rigid objects and relevance in Mixed Reality.

2. Implement the current state-of-the-art algorithm - Lepard ([Li & Harada, 2022](#)) - on industry leading Mixed Reality platform - Microsoft HoloLens 2 ([Ungureanu et al., 2020](#)).
3. Evaluate real-time 3D point cloud registration for deformable and non-deformable objects in uncontrolled real-world settings in the presence and absence of distraction and with varying levels of noise in the 3D scans.
4. Identify and mitigate any causes of drift or misalignment and potential bottlenecks slowing down the inference pipeline.

A.4 Background

In this section we will briefly introduce some important concepts that form the foundation of this thesis.

A.4.1 Mixed Reality

A.4.1.1 Introduction

Mixed Reality (MR) is a form of eXtended Reality (XR) that allows the user to render and interact with virtual 3D holograms in a real-world environment ([Rokhsaritalemi et al., 2020](#), [Speicher et al., 2019](#)). In an interior design use case, MR would allow the user to render the hologram of a couch in an empty room and move it around the room with hand gestures ([Huang et al., 2018](#)) to find out where in the room it would look best ([Jain & Werth, 2019](#), [Kent et al., 2021](#)). One of the primary use cases of this technology is to overlay or register a virtual reference model of an object on top of a real instance of the same object for comparison. For example, in manufacturing, a virtual reference model of a precision engineering part can be overlaid on a damaged instance for inspection, repair ([Abate et al., 2013](#), [Borsci et al., 2015](#)) and training ([Mueller & Ferreira, 2003](#), [Wang et al., 2004](#)). In remote assistance, a circuit diagram can be overlaid on a real switchboard and remote instructions can be issued for debugging the connections ([Ladwig & Geiger, 2018](#)). In surgery, pre-operative scans (like MRI, CT Scan, etc.) can be overlaid on the patient's organ in real-time for precise guidance to the point of surgery ([Chen et al., 2017](#)).

A.4.1.2 MR Headsets

The most important hardware component of a Mixed Reality system is the Head Mounted Display (HMD) or Headset. Some popular examples are Microsoft HoloLens [Ungureanu et al. \(2020\)](#) and Magic Leap. Mixed Reality headsets have a transparent visor through which the user can see the world and different kinds of optics and display elements that project the virtual objects in the field of view of the user. An elaborate set of RGB cameras and laser scanners is used for spatial mapping, localization and tracking. MR headsets also have an Inertial Measurement Unit (IMU) consisting of an accelerometer, a magnetometer and a gyroscope that tracks the movement of the user's head through space in six degrees of freedom. Figure A.1 shows the components of Microsoft HoloLens 2, the MR headset that we plan to use in this thesis. MR Headsets provide multi-modal user interfaces that combine head gestures, voice commands and eye gaze.

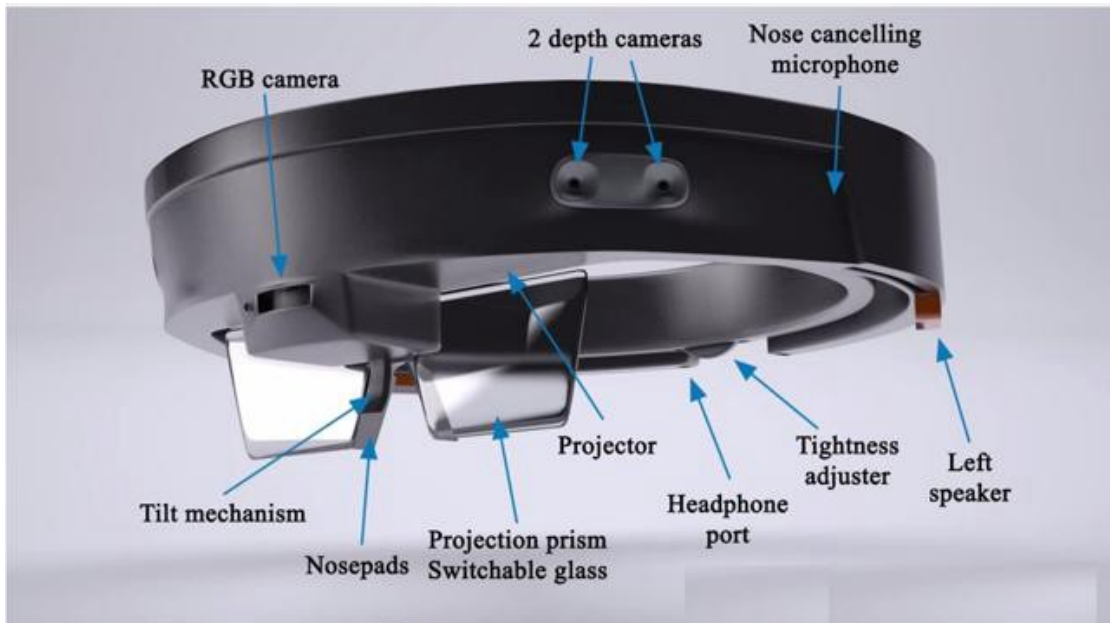


FIGURE A.1: Microsoft HoloLens 2, the Mixed Reality platform used in our study.

A.4.1.3 Challenges

MR headsets must be power efficient, lightweight and ergonomic. Spatial mapping using multiple modalities, scene reconstruction, gesture recognition, voice recognition, and high-polygon rendering are some primary tasks that are at the core of most Mixed Reality experiences. These 3D Computer Vision and Computer

Graphics tasks are compute-intensive and the limited on-device resources are not adequate for achieving these at a latency low enough for supporting an immersive MR experience. To mitigate this issue, most MR platforms employ a hybrid architecture where the compute-intensive tasks like those involving deep neural networks and rendering are off-loaded to high-performance and specialised hardware (e.g. GPU, FPGA) in the cloud and the on-board hardware is used only for encoding-decoding of data, communication with the cloud and interactions with the user (UX).

A.4.2 Point Cloud Registration

A.4.2.1 Introduction

Point cloud registration, also called Alignment (in MR jargon), is the task of finding a spatial transformation (such as rotation, transformation and scaling) which when applied to a source point cloud results in point-wise superposition with a destination point cloud of the same object/scene. These algorithms fall into two categories - rigid and non-rigid - depending on whether deformations in the object/scene between the two scans can be addressed.

A.4.2.2 Approaches to Solution

The general approach to point-cloud registration involves two steps: a) feature extraction, and b) feature matching and registration.

Feature extraction

Each point in a point cloud must be assigned a feature vector that represents its 3D position and context including local geometry, colour and texture (Weinmann et al., 2017). The first step is to define a neighbourhood for each point. Some common examples are spherical (Lee & Schenk, 2002, Linsen & Prautzsch, 2001) or cylindrical (Filin & Pfeifer, 2005, Niemeyer et al., 2014) neighbourhoods parameterized by radius (Filin & Pfeifer, 2005, Lee & Schenk, 2002) or the number of nearest neighbours by Euclidean distance (Linsen & Prautzsch, 2001, Niemeyer et al., 2014). These parameters give us the means to control the scale at which local 3D structures must be encoded. The value of the scale parameter is usually chosen using prior knowledge (Weinmann et al., 2015) or learned from data

(Demantké et al., 2011, Lalonde et al., 2005, Mitra & Nguyen, 2003, Weinmann et al., 2015) and multi-scale approaches are also popular (Brodu & Lague, 2012, Niemeyer et al., 2014, Schmidt et al., 2014). Once a neighbourhood of a point is defined, feature extraction encodes the local 3D geometry to attach semantics or context to the point. Certain shape primitives can be obtained by computing the eigenvalues of a 3D structure tensor constructed using the spatial coordinates of neighbouring points (Jutzi & Gross, 2009, Pauly et al., 2003, West et al., 2004). Other features that are extracted are angular characteristics (Munoz et al., 2009), height (Mallet et al., 2011), moments (Hackel et al., 2016), surface properties, slope, vertical profiles and 2D projections (Guo et al., 2015), shape distributions (Blomley et al., 2016, Osada et al., 2002), point-feature histograms (Rusu et al., 2009).

Modern approaches use Deep Neural Network (Goodfellow et al., 2016) based representation learning. Projection Networks project the 3D point cloud onto 2D image planes from multiple view-points and use 2D Convolutional Neural Networks (2D-CNN) (Goodfellow et al., 2016) to process them (Boulch et al., 2017, Lawin et al., 2017, Su et al., 2015). Voxel-based methods project the point cloud onto a 3D grid (Ben-Shabat et al., 2018, Maturana & Scherer, 2015, Roynard et al., 2018). Sparse data structures like octree and hash-maps are used for better efficiency and larger context sizes (Graham et al., 2018, Riegler et al., 2017). These grids are further processed using 3D Convolutional Neural Networks (3D-CNN) (Goodfellow et al., 2016). The main drawbacks of these approaches arise from the loss of details in the original point cloud structure during projection onto grids (Thomas et al., 2019). Graph Convolutional Networks address this problem by retaining the original position of each point and combining features on local surface patches (Verma et al., 2018, Wang et al., 2019). However, their representation is invariant to the deformations of those patches in Euclidean space which is not helpful for estimating non-rigid transformations between point clouds (Thomas et al., 2019). Pointwise Networks like PointNet (Qi et al., 2017) apply a shared neural network to each point followed by global max-pooling. This approach set new benchmarks in point-cloud classification and different variants using Multi-Layer Perceptron (MLP) [(Qi et al., 2017), (Li et al., 2018, Liu et al., 2019)] and CNN (Atzmon et al., 2018, Groh et al., 2018, Hua et al., 2018, Xu et al., 2018).

Kernel Point Convolution (KPConv) (Thomas et al., 2019) is one of the recent breakthroughs in point cloud representation learning and is particularly suitable

for deformable point clouds. It learns a kernel function to compute pointwise filters and increases representation power using deformable kernels. Instead of a grid-shaped kernel (as is the case with regular 2D and 3D CNNs), the kernel points in KPConv are spread freely in space. Each kernel point accumulates the features of the point-cloud points within a spherical neighbourhood around itself with weights that decay as the points get farther. In deformable KPConv, each kernel point also has a learnable offset that allows it to learn to adapt the shape of a kernel to different inputs. We will use KPConv to learn representations of our point clouds in the experiments for this thesis.

Feature matching and registration

After the points have been represented using feature vectors, the next task is to find corresponding points between the given pair of point clouds. Traditional methods use different variants of the RANdom-SAMple Consensus (RANSAC) algorithm for finding matching points (Holz et al., 2015, Schnabel et al., 2007). RANSAC is an iterative algorithm and works by classifying all possible correspondences into inliers and outliers. RANSAC is simple yet powerful and a bulk of the literature on point cloud registration uses RANSAC with both handcrafted and learned features (Ao et al., 2021, Bai et al., 2020, Choy et al., 2019, Deng et al., 2018a,b, El Banani et al., 2021, Yu et al., 2021, Zeng et al., 2017). For rigid point clouds, another popular algorithm is Iterative Closest Point (ICP) (Arun et al., 1987, Besl & McKay, 1992, Zhang, 1994). ICP assumes that the two point clouds are spatially close. In each iteration, for each point in the source point cloud, the closest point in the destination cloud is assigned as the matching point. Then the rigid transformation (rotation and translation) is computed by minimising mean-square loss. These steps are repeated till convergence. Direct Registration approaches combine feature extraction, feature matching and registration within a single architecture through end-to-end pose optimization (Aoki et al., 2019, Besl & McKay, 1992, Choy et al., 2020, Zhou et al., 2016).

Non-rigid correspondence has the added challenge of accounting for deformations. Different approaches have been proposed including projective correspondence (Newcombe et al., 2015), Siamese Network (Schmidt et al., 2016) and Scene Flow estimation (Li et al., 2021, Liu et al., 2019, Puy et al., 2020). Non-rigid correspondence is also studied in Geometry Processing where the input data is in the form of manifold surfaces. Methods like isometric deformation (Huang

et al., 2008), latent code optimization (Groueix et al., 2018) and functional maps (Ovsjanikov et al., 2012) have been studied in this context.

A.4.2.3 Challenges

Lack of ordering or structure

A point cloud is a collection of points in 3D space with no ordering or structure (like a grid). The absence of a grid structure makes it difficult to apply traditional deep learning methods like CNNs because they leverage the grid structure of their inputs (images/videos) for learning representations. As described in the previous section, there have been attempts (Ben-Shabat et al., 2018, Lawin et al., 2017, Maturana & Scherer, 2015, Roynard et al., 2018), to coerce/quantize/project point clouds to grids in order to harness the power of traditional CNNs while trading off the loss of the inherent structural details of the point cloud. New forms of convolution like KPConv (Thomas et al., 2019) also attempt to address this challenge with flexible non-grid kernels.

Sparsity

Most real-world 3D scans tend to be sparse A.2. As a result of this, a large amount of computing gets wasted processing zero entries. For efficient processing of sparse point clouds using Deep Neural Networks, the recently proposed Minkowski Engine (Choy et al., 2019) has proved to be a game changer. It represents point clouds as a position-indexed array and performs computation only for invalid regions. It can also leverage specialist hardware like GPU for greater throughput.

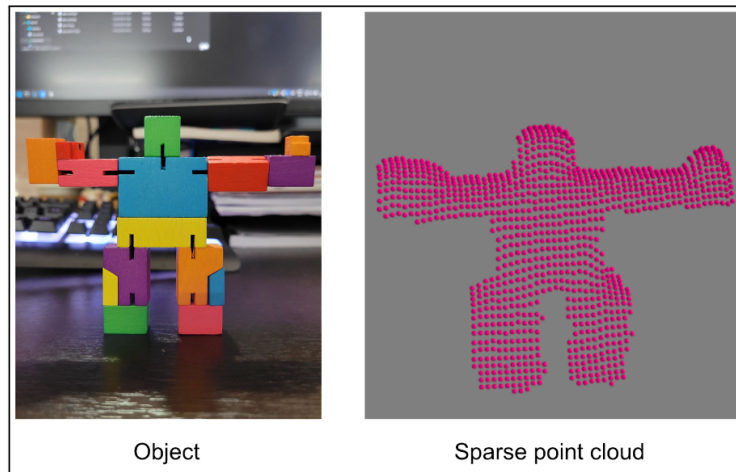


FIGURE A.2: Example of sparse point cloud scan

Noise and Outliers

Real-world 3D scans can be dirty with a large amount of noise and outliers [A.3](#). These are points that do not belong to the intended surface. One of the sources of outliers is a specular reflection from shiny surfaces like metal. In rigid registration, the RANSAC algorithm ([Holz et al., 2015](#), [Schnabel et al., 2007](#)) attempts to remove the outliers that do not conform with the model with maximum consensus. Learning approaches to outlier detection and removal include ([Bai et al., 2021](#), [Pais et al., 2020](#)).



FIGURE A.3: Example of noise in point clouds scanned by Microsoft HoloLens 2.

Partial Overlap

In a real-world use case of point cloud registration, the source and target point clouds may only have a partial match [A.4](#) albeit the fact that they are of the same object. This might be due to occlusion, object motion, or viewpoint change. A variety of methods have been proposed to perform the registration of point clouds that have a partial match ([Attaiki et al., 2021](#), [Rodolà et al., 2017](#), [Thomas et al., 2019](#), [Xu et al., 2021](#)).

A.5 Problem Statement

A.5.1 Definition

We use the same notation as the authors of *Lepard* in our paper. Let $\mathbf{S} \in \mathbb{R}^{n \times 3}$ be the source point cloud (with n points) and $\mathbf{T} \in \mathbb{R}^{m \times 3}$ be the target point cloud (with m points). Our goal is to calculate a warp function $\mathcal{W} : \mathbb{R} \rightarrow \mathbb{R}$ that maps \mathbf{S}

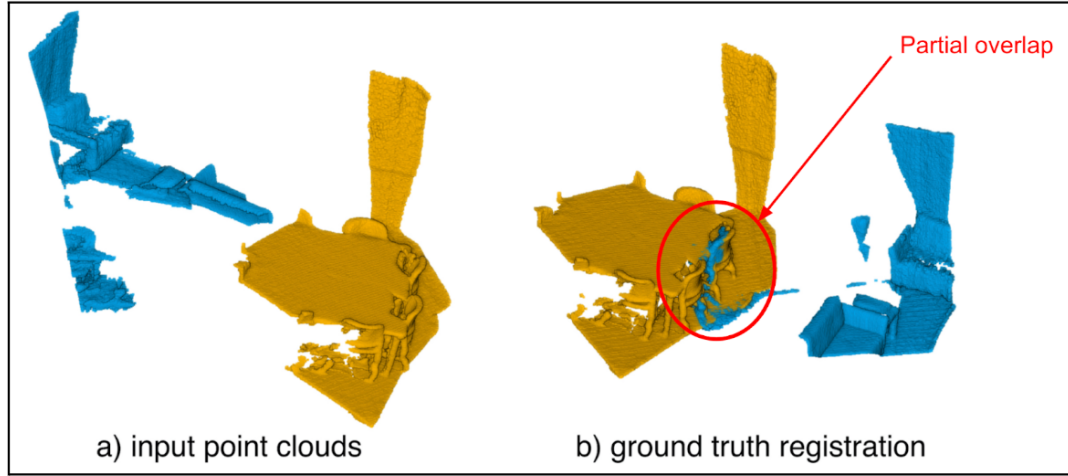


FIGURE A.4: Example of partial overlap between the source and target point clouds

to \mathbf{T} . For an arbitrary non-rigid deformation, \mathcal{W} generalizes to a dense per-point warp field. For the rigid case, \mathcal{W} can be parameterized as a $SE(3)$ transformation which is a single rotation and a single transformation applied to the whole body of \mathbf{S} .

A.5.2 Robust real-world performance

The system must be robust to real-world test conditions that contain noise and occlusion. For evaluation, we will collect data in cluttered environments using Microsoft Azure Kinect and Microsoft HoloLens 2.

A.6 Methodology

In this section, we describe our proposed research methodology.

A.6.1 Baseline Algorithm

We choose Leopard (Li & Harada, 2022) as our baseline algorithm as it is one of the current state-of-the-art methods for partial non-rigid point cloud registration. The algorithm uses powerful KPConv (Thomas et al., 2019) for learning deformable

point cloud representations. In order to add positional information to the translation invariant KPConv representation, the authors use Rotary Positional Encoding (Su et al., 2021). For point cloud matching it uses RANSAC algorithm (Holz et al., 2015, Schnabel et al., 2007) for rigid objects and deformable ICP for non-rigid objects. A transformer is used for position-aware feature matching and Rigid Fitting with Soft Procrustes (Arun et al., 1987) is used to obtain the final Rotation and Translation values for the transformation/warp function.

A.6.2 Training Objectives

The following are the loss functions used to train Lepard (Li & Harada, 2022):

1. **Matching Loss:** The Focal Loss over the confidence matrix returned by the matching layer is minimised.
2. **Warping Loss:** This is the L1 Loss between the target point cloud and the source point cloud warped by the Rotation and Translation matrices returned by the Procrustes layer.

A.6.3 Evaluation Metrics

The following are the metrics used for benchmarking point cloud registration algorithms:

1. **Inlier ratio (IR).** Inlier Ratio is the fraction of correct matches in the predicted correspondences set.
2. **Non-rigid Feature Matching Recall (NFMR).** NFMR measures the fraction of ground-truth matches that were successfully recovered by the correspondence prediction algorithm.

A.6.4 Datasets

We will consider training and fine-tuning our models on the following datasets. 3DMatch (Zeng et al., 2017) and 3DLoMatch (Huang et al., 2021) : These are

datasets for rigid-body partial point cloud registration consisting of indoor scans. 4DMatch and 4DLoMatch (Li & Harada, 2022): These are datasets for non-rigid partial point cloud registration derived from DeforminObjects4d (Li et al., 2021), a dataset of animated characters.

A.6.5 Real World Evaluation

4DMatch and 4DLoMatch (Li & Harada, 2022) are composed of animated objects. However, for real world use cases in Mixed Reality, Robotics, etc. we must evaluate the performance of non-rigid registration on noisy scans of real deformable objects. Figure A.5 shows a few test objects that we plan to use for evaluation in this project. Figure A.6 shows our test environment that is cluttered and represents a typical real-world usage environment of Mixed Reality devices.

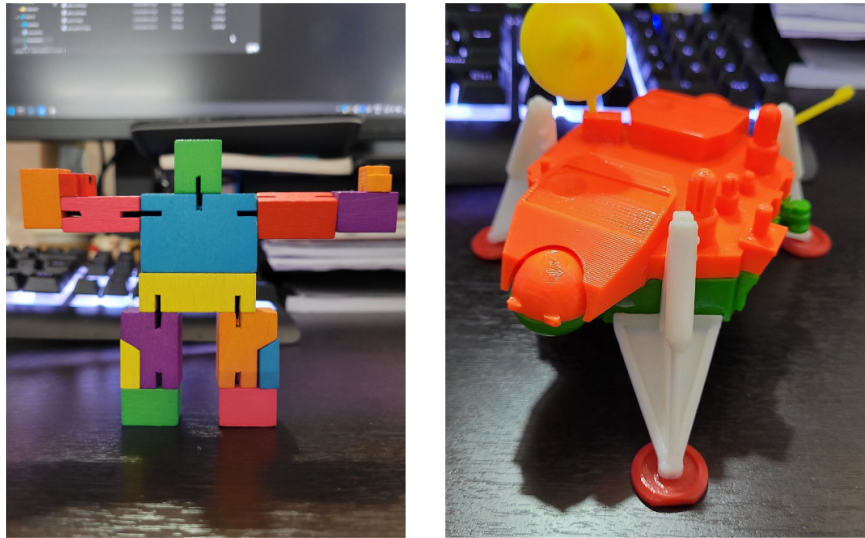


FIGURE A.5: Real-world objects used for our study. (Left) Cubebot robot model. (Right) Viking NASA Lander model.

A.7 Expected Outcome

Point cloud registration for non-rigid partial point clouds is a highly challenging computational problem. Although we focus on Mixed Reality applications in this thesis, the same approaches have profound significance in Indoor and Enterprise Robotics, Autonomous Driving, Unmanned Aerial Vehicles and Computer Graphics. Mixed Reality systems with non-rigid point cloud registration capabilities



FIGURE A.6: Real-world environment (cluttered) used in our tests.

can be used for remote maintenance and repair of deformable precision engineering components like cables, hoses and valves (Abate et al., 2013) and in medical science for rendering 3D diagnostic scans like CT and MRI over deformable and dynamic organs during surgery (Kersten-Oertel et al., 2013) - among others.

In this thesis we will implement a state-of-the-art point cloud registration algorithm - Lepard (Li & Harada, 2022) - on Microsoft HoloLens 2 Mixed Reality Platform (Ungureanu et al., 2020) and study the performance of the integrated system on a wide range of objects in real-world cluttered environments. We will study the failure modes and potential bottlenecks in the inference pipeline affecting latency and investigate the root causes. This study will enable us to develop an improved version of Lepard that is more robust to outliers and noise and has a fast inference pipeline for supporting real-time Mixed Reality applications.

A.8 Required Resources

The required resources for this thesis can be grouped into two categories: hardware and software.

A.8.1 Hardware

Training and inference using Deep Neural Networks with the Lepard architecture (Li & Harada, 2022) in a reasonable amount of time will require access to Graphics Processing Units or GPUs. I have access to two high-performance laptop computers with one GPU each. The following are the details:

TABLE A.1: Gantt Chart showing the plan of work for this thesis.

Task Name	August	September	October	November
Implementation of Lepard on HoloLens 2.				
Evaluation of rigid and non-rigid point cloud registration on custom data (HoloLens 2)				
Investigation of failure modes and mitigation				
Thesis writing				

- 2020 Lenovo Legion with RTX-2080 GPU
- 2016 Asus Republic Of Gamers with GTX-1080 GPU

I also have access to a blade server with Intel Xeon processors if any additional requirements arise during the project.

Since this thesis focuses on non-rigid alignment for Mixed Reality applications, I will need access to a MR headset. I have access to a 2022 Microsoft HoloLens 2 Enterprise Edition headset. For scanning 3D point clouds, I will use my HoloLens 2 and a Microsoft Azure Kinect camera that I also have access to.

A.8.2 Software

For implementing Lepard (Li & Harada, 2022), I will use the GitHub repository: <https://github.com/rabbityl/lepard> as starter code. Running point cloud registration on HoloLens 2 will require access to the HoloLens 2 Research Mode (Ungureanu et al., 2020) that I also have multiple years of experience in.

For evaluation of the quality of alignment, I will use CloudCompare (Girardeau-Montaut, 2016) and HoloLens 2 Spectator View that I also have access to.

A.9 Plan of Work

Table A.1 is a Gantt Chart with a time plan for the project considering November 25th, 2022 as the deadline for thesis submission.

A.9.1 Contingency Plan

The baseline algorithm that we have chosen - Lepard (Li & Harada, 2022) - is state-of-the-art. However, implementing it might take longer than expected. Since our

training setup is different from the authors', our results might not be in line with the ones that have been reported by the authors in the paper and this is a common problem with a lot of modern deep neural network based works. In that case, our contingency plan is to use a functional map based state-of-the-art baseline called SyNoRiM ([Huang et al., 2022](#)) that we already have working on our HoloLens 2 setup.